Eruptive history and ^{40}Ar/^{39}Ar geochronology of the Milos volcanic field, Greece

Xiaolong Zhou[1], Klaudia Kuiper[1], Jan Wijbrans[1], Katharina Boehm1, Pieter Vroon[1]

[1]Department of Earth Sciences, VU University Amsterdam, De Boelelaan 1085, 1081 HV Amsterdam, The Netherlands.

Correspondence to: Xiaolong Zhou (z.x.l.zhou@vu.nl)

Abstract. High-resolution geochronology is essential ~~to determine~~ the growth-rate of volcanoes, which is one of the key factors ~~to establish~~ the periodicity of explosive volcanic eruptions. However, there are less high-resolution eruptive histories (>10^6 years) determined for long-lived submarine arc volcanic complexes than for subaerial complexes, since ~~the~~ submarine volcanoes are far more difficult to observe than subaerial ones. In this study, high-resolution geochronology and major element data are presented for Milos Volcanic Field (VF) in the South Aegean Volcanic Arc, Greece. The Milos VF has been active for over 3 Myrs, and the first two million years of its eruptive history occurred in a submarine setting that has emerged above sea level ~~nowadays.~~ The long submarine volcanic history of the Milos VF makes it an excellent natural laboratory to study the growth-rate of a long-lived submarine arc volcanic complex. This study reports twenty-one new high-precision ^{40}Ar/^{39}Ar ages and major element compositions for eleven volcanic units of the Milos VF. This allows us to divide the Milos volcanic history into at least three periods of different long term volumetric volcanic output rate (Q_e). Period I (~3.3-2.36 Ma) and III (1.48 Ma-present) have low Q_e of $0.9 \pm 0.5 \times 10^{-5}$ km^3.yr^{-1} and $0.25 \pm 0.05 \times 10^{-5}$ km^3.yr^{-1}, respectively. Period II (2.36 - 1.48 Ma) has a 3-12 times higher Q_e of $3.0 \pm 1.7 \times 10^{-5}$ km^3.yr^{-1}. The Q_e of the Milos VF is 2-3 orders of magnitude lower than the average for rhyolitic systems and continental arcs. Most of the effusive eruptions of Period II are probably derived from magma chambers in the upper crust, whereas the more pumiceous units of Period I and III are probably related to lower crustal hot-zone.

1 Introduction

Short-term eruptive histories and compositional variations of lavas and pyroclastic deposits of many arc volcanic fields are well established. However, high-resolution eruptive histories that extend back > 10^5-10^6 years have been determined only for a handful of long-lived subaerial arc volcanic complexes. Some examples are: Mount Adams (Hildreth and Lanphere, 1994), Tatara–San Pedro (Singer et al., 1997), Santorini (Druitt et al., 1999), Montserrat (Cole et al., 2002), Mount Baker (Hildreth et al., 2003a), Katmai (Hildreth et al., 2003b), and Ceboruco–San Pedro (Frey et al., 2004). In order to establish the growth rate of volcanic complexes and to disentangle the processes which are responsible for the eruption, fractionation, storage and transport of magmas over time, comprehensive geological studies are required. These include detailed field mapping, sampling, high-resolution geochronology and geochemical analysis. Based on these integrated studies, the growth-rate of volcanoes can be determined to establish the periodicity of effusive and explosive volcanism.

The Milos Volcanic Field (VF) is a long-lived volcanic complex which has been active for over 3 Myrs. The Milos VF erupted for a significant part of its life below sea level, similar to the other well studied volcanic structures in the eastern Mediterranean (Fytikas et al., 1986; Stewart and McPhie, 2006). The eruptive history of the Milos VF has been examined with a broad range of the chronostratigraphic techniques such as K-Ar, U-Pb, fission track, ^{14}C and biostratigraphy (e.g. Angelier et al., 1977, Fytikas et al., 1976, 1986, Traineau and Dalabakis, 1989, Matsuda et al., 1999, Stewart and McPhie, 2006, Van Hinsbergen et al., 2004 and Calvo et al., 2012). However, most of the published ages have been measured using the less precise K-Ar or fission track methods, and modern, high precision ^{40}Ar/^{39}Ar ages for the Milos VF have not been published so far. In this study, (1) we provide high-precision ^{40}Ar/^{39}Ar geochronology of key volcanic units of the Milos VF and (2) refine the

stratigraphic framework of the Milos VF with the new high-precision $^{40}Ar/^{39}Ar$ ages and major element composition. (3) We also quantify and constrain the compositional and volumetric temporal evolution of volcanic products of the Milos VF.

1.1 Geological setting

The Milos VF is part of the South Aegean Volcanic Arc (SAVA), an arc which was formed in the eastern Mediterranean by subduction of the African plate beneath the Aegean microplate (Figure 1, Nicholls, 1971; Spakman et al., 1988; Duermeijer et al., 2000; Pe-Piper and Piper, 2007; Rontogianni et al., 2011). The present-day Benioff zone is located approximately 90 km underneath the Milos VF (Hayes et al., 2018). The upper plate is influenced by extensional tectonics (e.g. McKenzie, 1978; Pe-Piper and Piper, 2013), which is evident on the island of Milos as horst and graben structures (Figure 2).

The Milos VF is exposed on the islands of the Milos archipelago: Milos, Antimilos, Kimolos and Polyegos. The focus of this study is Milos with a surface area of 151 km^2 for the main island. The geology and volcanology of Milos have been extensively studied in the last 100 years. The first geological map was produced by Sonder (1924). This work was extended by Fytikas et al. (1976) and Angelier et al. (1977) and subsequent publications by Fytikas (Fytikas, 1989; Fytikas et al., 1986). Interpretations based on volcanic facies of the complete stratigraphy were made by Stewart and McPhie (Stewart and McPhie, 2003, 2006). More detailed studies of single volcanic centres (e.g. Bombarda volcano and Fyriplaka complex) were published by Campos Venuti and Rossi (1996) and Rinaldi et al. (2003). Milos has also been extensively studied for its epithermal gold mineralization, that has been summarized by Alfieris et al. (2013). Milos was known during the Neolithic period for its export of high quality obsidian. Today the main export product is kaolinite, that is mined from hydrothermally altered felsic volcanic units in the centre of the island (e.g. Alfieris et al. 2013).

The geology of Milos can be divided into four main units: (1) metamorphic basement, (2) Neogene sedimentary rocks, (3) volcanic sequences and (4) the alluvial cover. The metamorphic basement crops out at the southwest, south and southeast of Milos (Figure 3) and is also found as lithic blocks in many volcanic units. The metamorphic rocks include lawsonite-free jadeite eclogite, lawsonite eclogite, glaucophane schist, quartz-muscovite-chlorite and chlorite-amphibole schist (Fytikas et al., 1976, 1986; Grasemann et al., 2018; Kornprobst et al., 1979). The exposed units belong to the Cycladic Blueschist Unit (Lower Cycladic nappe), whereas eclogite pebbles in the green lahar unit (e.g. Fytikas, 1977) are derived from the Upper Cycladic Nappe (Grasemann et al., 2018).

On top of this metamorphic basement Neogene fossiliferous marine sedimentary rocks were deposited (e.g. Van Hinsbergen et al. 2004). This sedimentary sequence can be divided into a lower unit A and upper unit B that is unconformable overlain by volcaniclastic sediments (Van Hinsbergen et al., 2004). Unit A is 80 m thick and consists of fluviatile-lacustrine, brackish and shallow marine conglomerate, sandstone, dolomite and limestone. Unit B is 25-60 m thick and consists of a sandstone overlain by a succession of alternating marls and sapropels, suggesting a deeper marine setting (Van Hinsbergen et al., 2004). Five volcanic ash layers that contain biotite are found in this Neogene sedimentary rock sequence either suggesting that volcanic eruptions in small volume already occurred in the Milos area, or that these ash layers are derived from larger eruptions of volcanic centres further away from Milos (van Hinsbergen et al., 2004). Age determinations by bio-magneto- and cyclo-stratigraphy suggested that deposition of Unit A started at approximately 5 Ma, and that Milos subsided 900 m in 0.6 million years (Van Hinsbergen et al. 2004) due to extension. This subsidence happened ca 1.0-1.5 Myrs before the onset of the main phase of Pliocene- recent volcanism on Milos.

The Pliocene-recent volcanic sequence of Milos has been subdivided into different units by Angelier et al. (1977) and Fytikas et al. (1986). In addition, Stewart and McPhie (2006) provided a detailed facies analysis of the different volcanic units. The subdivision by Angelier et al. (1977) is not constrained well due to their limited amount of age data. The subdivision of volcanic units by Fytikas et al. (1986) and facies descriptions of Stewart and McPhie (2006) are summarized below. It is important to note that according to Stewart and McPhie (2006), the five volcanic cycles described by Fytikas et al. (1986) are difficult to match with existing age data and the continuous progression in volcanic construction (Fig. 4). For example, the first phase of

Fytikas et al. (1986), the Basal Pyroclastic Series, contains the large pumice cone-crypto dome volcanoes according to Stewart and McPhie (2006). Two of these pumice-cone crypto dome volcanoes are much younger and intercalated between the Complex of Domes and Lava Flows (CDLF) of Fytikas et al. (1986).

The first volcanic unit deposited in the Milos area is the Basal Pyroclastic Series (BPS) (Fytikas et al., 1986) or submarine felsic cryptodome-pumice cone volcanoes (Stewart and McPhie, 2006, Figure 2-4). This unit consist of thickly bedded pumice breccia with a rhyolitic-dacitic composition. These rhyolites-dacites are aphyric or contain quartz-feldspar±biotite phenocrysts. Graded sandstone and bioturbated and fossil rich (in-situ bivalve shells) mudstone are intercalated, indicating a marine environment and a water depth of several hundreds of meters (e.g. Stewart, 2003; Stewart and McPhie, 2006), whereas later degassed magmas with a similar composition intruded as sills and cryptodomes. The BPS has been strongly affected by hydrothermal fluids, especially the proximal deposits (e.g. Kilias et al., 2001).

The second volcanic unit was named the Complex of Domes and Lava Flows (CDLF, Fytikas et al., 1986) and the volcanic facies of this unit is described as the submarine dacitic and andesitic domes by Stewart and McPhie (2006). This phase of effusive submarine volcanism was predominantly andesitic/dacitic in composition and produced microcrystalline rocks with phenocrysts of pyroxene, amphibole, biotite and plagioclase. The eruption centres were mainly located along NNE faults and formed up to 300 m thick deposits extending over areas of 2.5 to 10 km around the eruption centres. In the north-eastern part of Milos, an andesitic scoria cone provided scoria lapilli and bombs to deeper water settings. Sandstone intercalated in the CDLF contains both igneous and metamorphic minerals suggesting input from the basement. Rounded pebbles of rhyolite and dacite indicate that some of the volcanic deposits were above sea level, or in very shallow, near shore environments (e.g. Stewart and McPhie, 2006).

The third volcanic unit is called the Pyroclastic Series and Lava Domes (PSLD) by Fytikas et al. (1986) and belongs to submarine-to-subaerial dacitic and andesitic lava domes of Stewart and McPhie (2006). This highly variable group is dominated by rhyolitic, dacitic and andesitic lavas, domes, pyroclastic deposits and felsic pumiceous sediments (Stewart and McPhie, 2006). Thickness varies between 50-200 m, and the deposits are located in the eastern and northern parts of Milos (Figure 2 and 3). The initial pyroclastic layers were subaqueously deposited and the extrusion of a dome resulted in deposition of talus around the margins by mass flow. On top of the dome sand- and siltstone with fossils (Ostrea fossil assemblage) and traction-current structures suggest that the top of the dome was above wave base. The youngest deposits of this unit are dacitic and andesitic lavas and domes. These domes generated subaerial block-and-ash flow and surge deposits. Paleosols within these deposits are a clear indicator that some areas were above sea level. The last unit of the PSLD is represented by large subaerial rhyolitic lava that contain quartz and biotite phenocrysts and is found near Halepa in the south-central part of Milos.

The fourth unit consists of the subaerially constructed rhyolitic Complexes of Trachilas and Fyriplaka (CTF) (Fytikas et al., 1986), which Stewart and McPhie (2006) interpreted as subaerial rhyolitic lava-pumice cones. These two volcanic complexes are built from rhyolitic pumice deposits and lavas that contain quartz and biotite phenocrysts (10-20 modal %). The deposits have a maximum thickness of 120 m and decrease to several meters thickness in the distal parts. Basement-derived schist is found as lithic clasts (Fytikas et al., 1986). In addition, the Kalamos rhyolitic lava dome that outcrops on the southern coast of Milos produced a lava that spread westwards to the Fyriplaka beach (Figure 2). This lava belongs to this fourth phase and is probably derived from an older volcano and not the Fyriplaka complex (Campos Venuti and Rossi, 1996).

The fifth volcanic unit comprises deposits from phreatic activity, especially in the northern part of the Zefiria Graben and near Agia Kiriaki (Figure 2 of Stewart and McPhie, 2006). Many overlapping craters are surrounded by lithic breccias that are composed of variably altered metamorphic basement clasts and volcanic clasts. This phreatic activity has continued into historic times (Trainau and Dalabakis, 1989). Fytikas et al. (1986) described this unit as "green lahar", although indicated that this deposit is not a lahar but the product of phreatic eruptions in the last 0.2 Ma.

1.2 Previous geochronological studies

Previous geochronological work is summarised in Table 1. Angelier et al. (1977) reported six K-Ar ages (0.95-2.50 Ma). These ages were used in combination with field observations to divide the Milos volcanic succession into four units. However, the samples from Fyriplaka, the fourth unit, were too young to be dated by Angelier et al. (1977). Fytikas et al. (1976, 1986) published 16 K-Ar ages for Milos (0.09-3.50 Ma) including an age of 0.09-0.14 Ma for the Fyriplaka complex. Fytikas et al. (1986) also obtained 3 K-Ar ages for Antimilos (0.32 ± 0.05 Ma), Kimolos (3.34 ± 0.06 Ma) and Polyegos (2.34 ± 0.17 Ma). Trainau and Dalabakis (1989) dated the very young phreatic deposits by ^{14}C dating and found ages between 200 BC and 200 AD. Matsuda et al. (1999) published two K-Ar ages of 0.8 ± 0.1 (MI-1) and 1.2 ± 0.1 Ma (MI-4) for the Plakes dome that was also studied by Fytikas et al. (1986). Bigazzi and Radi (1981) published two fission track ages of 1.54 ± 0.18 and 1.57 ± 0.15 Ma for obsidians of Bombarda-Adamas and Demenaghaki, respectively. Later fission track studies by Arias et al. (2006) (1.57 ± 0.12 and 1.60 ± 0.06 Ma) confirmed these ages. The fission track ages are younger than the K-Ar ages given by Angelier et al. (1977; 1.84 ± 0.08 Ma for Demenaghaki) and Fytikas et al. (1986; 1.71 ± 0.05 Ma for Bombarda). In the most recent geochronological study of the Milos VF, Stewart and McPhie (2006) published 4 SHRIMP U/Pb zircon ages: Triades dacite facies (1.44 ± 0.08 and 2.18 ± 0.09 Ma), Kalogeros cryptodome (2.70 ± 0.04 Ma) and the Fylakopi Pumice Breccia (2.66 ± 0.07 Ma). All uncertainties reported here are 1 standard deviation uncertainties as reported in the original publications, except for the ^{14}C ages for which uncertainties were not specified.

2 Methods

2.1 Mineral separation and sample preparation

Samples were collected from all major volcanic units on Milos island as based on the studies of Fytikas et al. (1986), Stewart and McPhie (2006) and our own observations in the field. Photos of the sample locations and thin sections can be found in the supplementary material I. Approximately 2 kg of fresh juvenile pyroclastic material or lava was sampled from each unit. Samples were cut ~in ~5 cm^3 cubes using a diamond saw to remove potentially altered surfaces and obtain the fresh interior parts. These cubes were ultra-sonicated for 30 minutes in demi-water to remove dust and seawater and dried in an oven overnight at 50 °C. Dry sample cubes were crushed in a steel jaw crusher, and this fraction was split into two portions of roughly equal size. One of them was powdered in an agate shatter box and agate ball mill to a grain size of less than 2 μm for the major-element analysis. The second fraction was sieved to obtain a grain size of 250-500 μm for ^{40}Ar/^{39}Ar dating. Heavy liquids density separation techniques (IJlst, 1973) were used to purify mineral separates (groundmass, biotite, amphibole) required for the ^{40}Ar/^{39}Ar dating. Different densities of heavy liquids were used to obtain groundmass (2700≤ρ≤3000 kg.m$^-$^{3}), biotite (2900≤ρ≤3100 kg.m^{-3}) and/or amphibole (~3100≤ ρ ≤3200 kg.m^{-3}). A Franz Isodynamic ~Magnet~ separator was used to remove the magnetic minerals from the non-magnetic minerals and groundmass. The samples for ^{40}Ar/^{39}Ar analysis were purified by handpicking under a binocular optical microscope to select mineral grains without visible alteration and inclusions.

2.2 ^{40}Ar/^{39}Ar dating

The mineral and groundmass samples were wrapped in either 6- or 9-mm aluminium foil and packed in 20 mm aluminium cups, that were vertically stacked. Based on stratigraphy and previous geochronological constraints >1 Ma samples and the <1 Ma samples were irradiated for ~respectively~ 7 and 1 hours in irradiation batches VU108 and VU110 in the CLICIT facility of the OSU TRIGA reactor. The neutron flux for all irradiations was monitored by standard bracketing using the Drachenfels sanidine (DRA; 25.52 ± 0.08 Ma, modified from Wijbrans et al., 1995 and calibrated relative to Kuiper et al., 2008) and Fish Canyon Tuff sanidine (FCs; 28.201 ± 0.023 Ma, Kuiper et al., 2008) with Min et al. (2000) decay constants.

In total 24 samples (8 groundmasses, 15 biotites and 2 amphiboles, for sample G15M0026 both biotite and amphibole were analysed) were measured by either $^{40}Ar/^{39}Ar$ fusion and/or incremental heating techniques. For incremental heating experiments 80-100 grains per sample were loaded into a 25-hole (surface per hole ~36 mm^2) copper tray together with single grain standards in ~12 mm^2 holes. The tray was prebaked in vacuum (10^{-5}-10^{-6} mbar) at 250 °C overnight to remove atmospheric argon and subsequently baked overnight at 120 °C in the ultra-high vacuum sample chamber ($<5*10^{-9}$ mbar) and purification system connected to a Thermo Scientific Helix MC mass spectrometer.

Samples and standards were heated with a focused laser beam at 8 % power using a 50W CW CO_2 laser. The released gas was cleaned by exposure to a cold trap cooled by a Lauda cooler at -70 °C, a SAES NP10 at 400 °C, Ti sponge at 500 °C and cold SAES ST172 Fe-V-Zr sintered metal. The five isotopes of argon were measured simultaneously on five different collectors: ^{40}Ar on the H2-Faraday, ^{39}Ar on the H1-Faraday or the H1-CDD, ^{38}Ar on the AX-CDD, ^{37}Ar on the L1-CDD and ^{36}Ar on the L2-CDD for 15 cycles with 33 seconds integration time (CDD: compact discrete dynodes). The Faraday cups on H2 and H1 were equipped with 10^{13} Ohm amplifiers. Procedural blanks were measured every 2 or 3 analyses in different sequences, and air-shots were measured every 8-12 hours to correct the instrumental mass discrimination. Gain between different collectors was monitored by measuring CO_2 on mass 44 in dynamic mode on all collectors. Gain was generally stable over periods of weeks. Note, that because samples, standards and air calibration runs are measured during the same period, gain correction does not substantially change the final age results. The raw mass spectrometer data output was converted by an in-house designed Excel macro script to be compatible with the ArArCalc 2.5 data reduction software (Koppers, 2002).The atmospheric air value of 298.56 from Lee et al. (2006) is used in the calculations. The correction factors for neutron interference reactions are (2.64 ± 0.02) x10^{-4} for $(^{36}Ar/^{37}Ar)_{Ca}$, (6.73 ± 0.04) x10^{-4} for $(^{39}Ar/^{37}Ar)_{Ca}$, (1.21 ± 0.003) x10^{-2} for $(^{38}Ar/^{39}Ar)_K$ and (8.6 ± 0.7) x10^{-4} for $(^{40}Ar/^{39}Ar)_K$. All uncertainties are quoted at the 1σ level and include all analytical errors (i.e. blank, mass discrimination and neutron interference correction and analytical error in J-factor, the parameter associated with the irradiation process).

A reliable plateau age is defined as experiments with at least 3 consecutive steps overlapping at 2-sigma, containing >50% of the $^{39}Ar_K$, a Mean Square Weighted Deviate (MSWD) value<2.5, and with an $^{40}Ar/^{36}Ar$ inverse isochron intercept that does not deviate from atmospheric argon at 2-sigma. All the inverse isochron ages used the same steps as used in the weighted mean ages, and all relevant analytical data for the age calculations following standard practices (Schaen et al., 2020) can be found in in the supplementary material II.

2.3 Whole-rock major element analysis by XRF

Major-element concentrations were measured by X-ray fluorescence spectroscopy (XRF) on a Panalytical AxiosMax. A Panalytical Eagon2 was used to create 40mm fused glass beads of $Li_2B_4O_7/LiBO_2$ (65.5:33.5%, Johnson & Johnson Spectroflux 110) with a 1:6 dilution sample-flux ratio that were molten at 1150 °C. Sample powders were ignited at 1000 °C for 2 hours to determine loss on ignition (LOI) before being mixed with the $Li_2B_4O_7/LiBO_2$ flux. Interference corrected spectra intensities were converted to oxide-concentrations against a calibration curve consisting of 30 international standards. The precision, expressed as the coefficient of variation (CV), is better than 0.5%. The accuracy, as measured on the international standards AGV-2, BHVO-2, BCR-2 and GSP-2 was better than 0.7% (1 RSD) (supplementary material III).

2.4 Rock textural analysis and eruption volume calculations

The crystallinity and vesicularity were estimated with Image-J software by scanning the thin section of each sample 4-6 times to cover the entire area. For the crystallinity only the phenocrysts were considered, crystals smaller than 50 μm were included in the groundmass. The estimations of crystallinity and vesicularity on the older samples (>1.0 Ma) of Milos VF are all from lava and domes. The younger samples (<1.0 Ma) are from pumiceous pyroclastic units. The other old pumices of the Profitis Illias and Filakopi volcanoes are not included in this study due to the severe alteration that prevents the collection of reliable

geochemical and geochronological data on these samples. The mean value and standard deviation of the crystallinity and vesicularity were also calculated.

The minimum and/or maximum eruption volume of each volcano during each eruption period is derived from the ranges of thickness and surface areas that are reported in Campos and Rossi (1996) and Stewart and McPhie (2006). We converted these volumes to Dense Rock Equivalent (DRE) based on the magma type of different deposits. This analysis only includes the onshore deposits and results in a smaller estimate for larger pyroclastic volumes. The DRE volume is calculated using the equation of (Crosweller et al., 2012):

$$DRE\ (km^3) = \frac{tephra\ vol\ (km^3) \times tephra density\ (kg/m^3)}{magma\ density\ (kg/m^3)}$$

Tephra density is assumed to be 1000 kg/m^3 (Crosweller et al., 2012). Magma density varies depending on the magma type. Here we used 2300 kg/m^3 for rocks with a SiO$_2$ range of 65-77 wt.% and 2500 kg/m^3 for all samples with SiO$_2$ < 65 wt.% (Table 4 for major-element composition). DRE corresponds to the unvesiculated erupted magma volume and DRE volumes are converted to include vesicularity. Therefore, we did not convert the volume of some cryptodome and lavas from Profitis Illias (G15M0017), Triades (G15M0021-24), Dhemeneghaki (G15M0032B) and Halepa (G15M0013) to the DRE since they contain less than 5% vesicles.

3 Results

3.1 ^{40}Ar/^{39}Ar age results

In this section, we present our groundmass, biotite and amphibole ^{40}Ar/^{39}Ar results for eleven volcanic units of Milos. The ^{40}Ar/^{39}Ar ages range from 0.06 to 4.10 Ma and cover most of the major volcanic units of Milos. Table 2 and 3 show the ^{40}Ar/^{39}Ar results of incremental heating steps and single grain fusion analyses, respectively. Note that the Irr-ID column in these two Tables represents the irradiation ID of the analytical experiment (e.g. VU108-, VU110-) and the top right superscripts (G, B, A, O) in the sample IDs (e.g., G15M0029^G, G15M0021^B) refer to groundmass, biotite, amphibole and obsidian.

3.1.1 Groundmass ^{40}Ar/^{39}Ar plateau and/or isochron ages

All groundmass samples yielding ^{40}Ar/^{39}Ar plateau and isochron ages with more than 50% ^{39}Ar$_K$ and less than 2.5 MSWD included in their age spectrum are shown in Figure 4 and reported in Table 2. The ^{40}Ar/^{36}Ar isochron intercepts do not deviate from atmospheric argon at the 2-sigma level, unless stated otherwise (Table 3). Sample G15M0016 was collected from a dyke at Kleftiko in the southwest of Milos (Figure 2). Three incremental heating experiments were performed on the groundmass of this sample (Figure 5A). The first experiment (VU108-Z8a) produced a weighted mean age of 2.71 ± 0.02 Ma (MSWD 2.31; ^{39}Ar$_K$ 79.6%; inverse isochron age 2.65 ± 0.10 Ma). The other two, VU108-Z8a_4 and VU108-Z8b_1, have plateau ages of 2.61 ± 0.03 Ma (MSWD 0.93; ^{39}Ar$_K$ 57.4%; inverse isochron age 2.69 ± 0.10 Ma) and 2.67 ± 0.01 Ma (MSWD 1.50; ^{39}Ar$_K$ 65.57%; inverse isochron age 2.55 ± 0.05 Ma), respectively. The three experiments are remarkably similar. Although the amount of radiogenic ^{40}Ar is low (<20%), a combined age of 2.66 ± 0.01 Ma is considered to be best estimate with a relatively high MSWD value (2.51).

Two lava samples, G15M0019 and G15M0020, were collected from Kontaro in north-eastern Milos (Figure 2). Three replicate incremental heating steps experiments of groundmass from sample G15M0019 (VU108-Z6a_4; VU108-Z6a_5 and VU108-Z6b_1, Figure 5B) were performed that are not reproducible. Their plateau ages range from 1.55 Ma to 1.62 Ma with relatively high MSWD (3.8-4.5), 56-95% of the total ^{39}Ar$_K$, 34-53% of radiogenic ^{40}Ar, 0.88-1.02 of K/Ca and an atmospheric isochron intercept of 297-315. We consider the isochron age from the last experiment (VU108-Z6b_1) as the only reliable age (1.48 ± 0.02 Ma, MSWD 0.44) because of the least scatter in this experiment, and therefore the best estimate for the eruption age. Three replicate incremental heating steps experiments of groundmass from sample G15M0020 (VU108-Z5a_5; VU108-Z5b_1

242 and VU108-Z5b_2, Figure 5C) were analysed. These experiments are similar at the lower temperature heating steps. They

243 produced statistically meaningful plateau ages ranging from 1.52-1.56 Ma with 41-62% of the total $^{39}Ar_K$, 18-48% of

244 radiogenic ^{40}Ar, 1.51-1.73 of K/Ca and an atmospheric isochron intercept of 295-300. Their combined weighted mean age is

245 1.54 ± 0.01 Ma (MSWD 3.06; $^{39}Ar_K$ 57.32%) with 25.31% of $^{40}Ar^*$.

246 Sample G15M0032B (obsidian) was collected from a pumice cone volcano at Demeneghaki (Figure 2). One incremental

247 heating experiment of this sample (VU108-Z18, Figure 5D) yielded a plateau age of 1.825 ± 0.002 Ma (MSWD 0.91; $^{39}Ar_K$

248 98.6%). The $^{40}Ar^*$ is 93.86%. The inverse isochron age is identical to the weighted mean plateau age 1.825 ± 0.002 Ma. The

249 age of 1.825 ± 0.002 Ma is considered the best estimate for the eruption age of the Demeneghaki obsidian.

250 **3.1.2 Groundmass $^{40}Ar/^{39}Ar$ plateau and/or isochron ages (25-40% $^{39}Ar_K$ released)**

251 The results shown in Figure 5 did not yield weighted mean plateau according to standard criteria including $^{39}Ar_K > 50\%$, but

252 still provide some useful age information. Sample G15M0017 was collected from a cryptodome of the Profitis Illias volcano

253 of southwestern Milos (Figure 2). Three replicate incremental heating experiments, VU108-Z7a, VU108-Z7a_4 and VU108-

254 Z7b_1, have been performed on this sample which resulted in disturbed age spectra (Figure 6A). The consecutive lower

255 temperature steps of all experiments define ages of <2.5 Ma, which is much younger than the ages of the submarine pyroclastic

256 products of the lower series at Kleftiko and/or Profitis Illias (3.0-3.5 Ma, Fytikas et al., 1986 and Stewart and McPhie, 2006).

257 At the consecutive higher temperature heating steps, these experiments yielded 3.64 ± 0.08 Ma ($^{40}Ar/^{36}Ar$ 293.87 ± 4.77;

258 VU108-Z7a), 4.10 ± 0.06 Ma ($^{40}Ar/^{36}Ar$ 298.44 ± 15.51; VU108-Z7a_4) and 3.41 ± 0.05 Ma ($^{40}Ar/^{36}Ar$ 295.97 ± 7.34; VU108-

259 Z7b_1). The total fusion and inverse isochron ages of the three experiments gave large ranges of 2.25-3.23 and 3.68-4.14 Ma,

260 respectively, and none of these high temperature heating steps produced a statistical plateau (all MSWD > 2.0). The amount

261 of radiogenic ^{40}Ar of both $^{40}Ar/^{39}Ar$ result from our sample and K-Ar from previous studies (Fytikas et al., 1986) is rather low

262 (<15%) for a sample of this age based on our laboratory experience. Therefore, the estimated age range for the oldest volcanic

263 products of the Milos VF should be confirmed by other dating techniques.

264 Sample G15M0015 is also a cryptodome breccia from Profitis Illias (Figure 2). Two replicate incremental step heating

265 experiments were performed on the groundmass of this sample (VU108-Z9a and VU108-Z9b_1, Figure 6B). Experiment

266 VU108-Z9a groundmass shows a disturbed age spectrum with ages increasing from ~3 Ma in the initial heating steps to ~3.2

267 Ma followed by a decrease to ~3 Ma in the high temperature heating steps. The consecutive heating steps only exist at the

268 lower temperature steps yielding a "plateau" of 3.12 ± 0.02 Ma (MSWD 9.07). Due to the excess argon ($^{40}Ar/^{36}Ar$ 304.19 ±

269 1.25 comprising 43.07% of the released $^{39}Ar_K$), the inverse isochron of 3.06 ± 0.02 Ma (MSWD 0.01) is more reliable for this

270 analysis. The inverse isochron age of the second groundmass (VU108-Z9b_1) is identical at 3.04 ± 0.02 Ma (MSWD 1.14;

271 $^{39}Ar_K$ 27.00%) and $^{40}Ar/^{36}Ar$ of 293.83 ± 1.38 obtained at high temperature steps. The two experiments are remarkably similar.

272 Although the sample does not formally fulfil the definition of a plateau age comprising >50% $^{39}Ar_K$ released, a combined age

273 of 3.06 ± 0.02 Ma (MSWD 1.14; $^{39}Ar_K$ 22.79%, $^{40}Ar^*$ 41.77%) most likely represents the eruption age. This $^{40}Ar/^{36}Ar$ age is

274 consistent with the K-Ar age from the same lithology of 3.08 ± 0.08 Ma (Fytikas et al. 1986).

275 Sample G15M0029 is an andesite collected from Korakia in the northeast of Milos (Figure 2). Two incremental heating

276 experiments (VU108-Z16a and VU108-Z16b_1, Figure 6C) were performed on this sample. The two experiments are

277 remarkably similar with a decreasing age from ~2.85 Ma at the lower temperature heating steps to 2.65 Ma at the higher

278 temperatures. The higher temperature heating steps of both experiments yielded weighted mean plateau ages of 2.67 ± 0.01

279 Ma (MSWD 0.96; $^{39}Ar_K$ 23.61%, $^{40}Ar^*$ 56.34%; inverse isochron age 2.68 ± 0.02 Ma) and 2.69 ± 0.01 Ma (MSWD 1.32;

280 $^{39}Ar_K$ 27.08%, $^{40}Ar^*$ 55.78%; inverse isochron age 2.67 ± 0.03 Ma). The isochron intercepts for both experiments are

281 atmospheric. The combined age of 2.68 ± 0.01 Ma should be considered with caution due to the rather low amount of released

282 ^{39}Ar (23-28%).

3.1.3 Single biotite grain $^{40}Ar/^{39}Ar$ fusion and/or isochron ages

Results of nine single fusion experiments are given in Figure 7. Nine or ten replicate single fusion experiments were conducted on 5-10 grains biotite per fusion. Sample G15M0006 is from a solid in-situ dacite with columnar joints from the Kalogeros cryptodome in the northeast of Milos (VU108-Z11, Figure 7A). The sample shows a weighted mean age of 2.72 ± 0.01 Ma with 9 out of 10 total fusion experiments (MSWD 1.95; 9/10) with an average 47.9% of radiogenic ^{40}Ar. The inverse isochron age is 2.62 ± 0.04 Ma (MSWD 0.99). Note that excess argon ($^{40}Ar/^{36}Ar$ 310.2 ± 4.0) is present, hence the inverse isochron age is younger compared to the weighted mean age. The isochron age of 2.62 ± 0.04 Ma is considered as the best estimate for the emplacement age.

Sample G15M0025 was collected from the Mavros Kavos lava dome located in the west of Milos (Figure 2). The biotite of this sample (VU108-Z2, Figure 7B) shows a weighted mean age of 2.36 ± 0.01 Ma (MSWD 0.70; 9/10; $^{40}Ar*$ 37.60%, inverse isochron age 2.34 ± 0.04 Ma) with an $^{40}Ar/^{36}Ar$ intercept of 300.6 ± 3.5. The age of 2.36 ± 0.01 Ma is considered the best eruption age estimate for this sample.

Sample G15M0023 and -24 are from the Triades lava dome ~~of the~~ northeast of Milos (Figure 2). A mafic enclave G15M0022 (host rock G15M0021) was collected from a lava near Cape Vani (Figure 2). The total fusion experiments of the biotites show that their initial $^{40}Ar/^{36}Ar$ estimates overlap with air (296-300). The total fusion ages gave the best estimates for their eruption ages of 2.10-2.13 Ma using 22 out of 31 fusions with a range of radiogenic ^{40}Ar between 30-36% (Figure 7B).

Sample G15M0013 is from the rhyolitic Halepa lava dome in the south of Milos (Figure 2). The total fusion experiment (VU108-Z13, Figure 7C) on biotite of this sample produced a weighted mean age of 1.04 ± 0.01 Ma (MSWD 1.62; 9/10, $^{40}Ar*$ 26.3%; inverse isochron age 1.02 ± 0.04 Ma) with an initial $^{40}Ar/^{36}Ar$ estimate of 299. 8 ± 4.1. The best estimate for the eruption age of the Halepa rhyolite is 1.04 ± 0.01 Ma.

Sample G15M0034 and 35 were collected from a lava dome located southeast of the Trachilas cone (Figure 2). Nine total fusion experiments (VU108-Z21, Figure 7C) were performed on biotite of sample G15M0035 and yielded 0.63 ± 0.02 Ma (MSWD 1.26; 6/9; $^{40}Ar*$ 4.9%; inverse isochron age 0.77 ± 0.13 Ma). The atmospheric isochron intercept overlaps with air at 2-sigma (296.4 ± 1.7). The 4.9% of radiogenic ^{40}Ar is so low that we should consider the age of 0.63 ± 0.02 Ma with caution. For biotite of sample G15M0034 (VU108-Z20, Figure 7C) one total fusion experiment produced a weighted mean age of 0.51 ± 0.02 Ma (MSWD 0.95; 6/10; $^{40}Ar*$ 3.5%; inverse isochron age 0.61 ± 0.08 Ma) with an atmospheric isochron intercept. The age of 0.51 ± 0.02 Ma also needs to be considered as possibly suspect due to the low amount of radiogenic ^{40}Ar.

Sample G15M0033 was collected from the Kalamos lava along the coast of the southwest of the Fyriplaka rhyolitic complex (Figure 2). Biotite of this sample (VU108-Z19, Figure 7C) yielded 0.412 ± 0.004 Ma (MSWD 1.10; 8/10; inverse isochron age 0.39 ± 0.02 Ma) with ~22.2% of radiogenic ^{40}Ar which is considered as the eruption age for the Kalamos lava.

3.1.4 Multiple biotite grain $^{40}Ar/^{39}Ar$ incremental heating plateau and/or isochron ages

Figure 8 displays the biotite $^{40}Ar/^{39}Ar$ ages measured by the incremental heating steps method. Sample G15M0021 is the host lava of mafic enclave G15M0022. Twelve replicate total fusion experiments of its biotite (VU110-Z4, Table 3) produced an age of 2.48 ± 0.04 Ma (MSWD 1.49; 4/12, $^{40}Ar*$ 36.09%; inverse isochron age 3.44 ± 0.46 Ma). Although this suggests a correct age, the large analytical error of each fusion (>0.3 Ma on average) and poor reproducibility (4/12) of this experiment probably results in an unreliable age. Therefore, two more incremental heating experiments were performed on this sample (VU110-Z4_2 and VU110-Z4_2b, Figure 8A), that gave an age of 1.97 ± 0.01 Ma (MSWD 1.66; $^{39}Ar_K$ 63.8%, $^{40}Ar*$ 54.7%; inverse isochron age 1.97 ± 0.03 Ma) and 2.01 ± 0.01 Ma (MSWD 6.76; $^{39}Ar_K$ 75.39%, $^{40}Ar*$ 57.84%; inverse isochron age 2.04 ± 0.05 Ma), respectively. The scatter in the latter is too high to define a reliable plateau age and the first incremental heating experiment is considered as the best estimate of the eruption age of this sample.

Sample G15M0007 was collected from the rhyolitic Trachilas complex in the north of Milos (Figure 2). Twenty-two total fusion (VU110-Z12, Table 3) and two incremental heating experiments (VU110-Z12a and 12b, Figure 8B) were performed

on biotite of this sample. The total fusion experiments did not result in a reliable age due to the large errors of single steps ($\pm$ 0.19 Ma on average) and the rather low amount of radiogenic ^{40}Ar (9.1%). On the other hand, the first incremental heating experiment produced a plateau age of 0.30 $\pm$ 0.01 Ma (MSWD 4.61; $^{39}Ar_K$ 56.60%; inverse isochron age 0.28 $\pm$ 0.05 Ma) including 14.51% of radiogenic ^{40}Ar. The second incremental heating experiment yielded a plateau of 0.317 $\pm$ 0.004 Ma (MSWD 1.29; $^{39}Ar_K$ 74.05%; inverse isochron age 0.31 $\pm$ 0.03 Ma) with a higher amount of radiogenic ^{40}Ar (18.30%). The isochron intercepts of both incremental heating experiments are atmospheric. The second experiment is the best estimate for the eruption age, since it contained the largest amount of radiogenic ^{40}Ar and has a better reproducibility of single heating steps.

Three pumice clasts (G15M0008-9 and G15M0012) were sampled from different layers of the Fyriplaka complex (Figure 2). The first incremental step heating experiment of biotite from sample G15M0009 (VU110-Z23a, Figure 8C) gave negative ages at the lower temperature heating steps. Four consecutive higher temperature heating steps seem to define a "plateau" of 0.11 $\pm$ 0.02 Ma (MSWD 1.37) only using 18.33% of the total $^{39}Ar_K$ with 1.65% of radiogenic ^{40}Ar. The second experiment (VU110-Z23b) also yielded a "plateau" of 0.11 $\pm$ 0.03 Ma (MSWD 6.77) at higher temperature heating steps including 41.05% of the total $^{39}Ar_K$ and 3.13% of radiogenic ^{40}Ar. The significantly larger error of the isochron age may be due to the clustering of data close to zero on the y-axis. The two experiments (VU110-Z23a and Z23b) are comparable. The combined age of 0.11 $\pm$ 0.02 (MSWD 3.5) is consistent with the age of 0.09-0.14 Ma from Fytikas et al. (1986). Although only 29.50% of the released $^{39}Ar_K$ was used for this sample, we believe this age is the eruption age of this layer in the Fyriplaka complex.

For biotite of sample G15M0012 both incremental step heating experiments are comparable. Both of them yielded plateau ages of 0.05 $\pm$ 0.01 Ma (VU110-Z24a; MSWD 3.09; $^{39}Ar_K$ 38.89%, $^{40}Ar^*$ 2.89%; inverse isochron age 0.14 $\pm$ 0.03 Ma) and 0.09 $\pm$ 0.02 Ma (VU110-Z24b; MSWD 8.16; $^{39}Ar_K$ 48.04%, $^{40}Ar^*$ 4.59%; inverse isochron age 0.09 $\pm$ 0.05 Ma) at higher temperature heating steps (Figure 8C). The clustering of data points of experiment VU110-Z24a could result in the lower initial estimate of $^{40}Ar/^{36}Ar$ (285.98 $\pm$ 4.76). However, the combined age of 0.07 $\pm$ 0.01 Ma, using 43.53% of the total $^{39}Ar_K$ with an atmospheric isochron intercept (295.67 $\pm$ 7.39), could be the representative age of eruption.

Biotite of sample G15M0008 did not result in a reliable plateau in the first incremental step heating experiment (VU110-Z22a, Figure 8C) but shows a very disturbed age spectrum. The second experiment (VU110-Z22b) yielded 0.062 $\pm$ 0.003 Ma (MSWD 0.91) using 71.81% of the total $^{39}Ar_K$ with 2.69% of radiogenic ^{40}Ar as the best estimate of the eruption age.

3.1.5 Multiple amphibole grain $^{40}Ar/^{39}Ar$ multi-grain incremental heating plateau and/or isochron ages

There are only two amphibole samples that yielded $^{40}Ar/^{36}Ar$ plateau and/or isochron ages (Figure 9A and B). Sample G15M0004 was collected from the pyroclastic series of Adamas from the PSLD (Fytikas et al., 1986), to the north of Bombarda (Figure 2). Two replicate heating experiments of G15M0004 amphibole (VU108-Z10_1 and VU108-Z10_2) were performed yielding 2.99 $\pm$ 0.11 Ma (MSWD 1.00; $^{39}Ar_K$ 87.31%, $^{40}Ar^*$ 16.36%; inverse isochron age 7.89 $\pm$ 2.46 Ma) and 2.86 $\pm$ 0.09 Ma (MSWD 1.50; $^{39}Ar_K$ 86.18%, $^{40}Ar^*$ 17.58%; inverse isochron age 0.70 $\pm$ 0.29 Ma). The variable atmospheric isochron intercept of both experiments ($^{40}Ar/^{36}Ar$ 202.39 $\pm$ 48.47 and 348.91 $\pm$ 27.33) is due to clustering of the data points. Note that also the amount of radiogenic ^{40}Ar is rather low (~17%). The two experiments are remarkably similar. A combined inverse isochron age of 1.95 $\pm$ 0.45 Ma (MSWD 1.17; $^{40}Ar/^{36}Ar$ 319.51 $\pm$ 14.70) is considered the best estimate, but ideally this age should be checked by other techniques.

Sample G15M0026 is from the same location as sample G15M0025, which gives us the opportunity to compare the biotite age with the amphibole age. One total fusion experiment of biotite (VU108-Z1b) yielded a weighted mean age of 2.35 $\pm$ 0.01 Ma (MSWD 1.36; $^{40}Ar^*$ 38.6%). The atmospheric isochron intercept is low ($^{40}Ar/^{36}Ar$ 292.01 $\pm$ 2.92), the inverse isochron age of 2.42 $\pm$ 0.04 Ma (MSWD 0.93) is considered the best result from the biotite. Two incremental heating experiments for amphibole (VU108-Z1b_1 and VU108-Z1b_2) gave plateau ages of 2.67-2.70 Ma which are much higher values than the biotite inverse isochron ages (2.28-2.31 Ma). This result could be caused by the high $^{40}Ar/^{36}Ar$ isochron intercepts (>320) with

367 large uncertainties of ~29. Therefore, on the basis of the remarkable similarity of the two experiments, the combined inverse

368 isochron age of 2.31 ± 0.28 Ma (MSWD 0.93, $^{39}Ar_K$ 71.36%, $^{40}Ar^*$ 34.97%) is considered as the best estimate from amphibole

369 which overlaps with the biotite age of 2.42 ± 0.03 Ma. This biotite age of 2.42 ± 0.03 Ma is considered to the best approximation

370 of the eruption age.

3.2 Major element results

372 Major-element results are given in Table 4. The major element compositions range from 54 to 78 wt.% SiO_2 (basaltic-andesite-

373 rhyolite to dacite-rhyolite, see Figure 10A). The most felsic samples (SiO_2>75 wt.%) belong to the Fyriplaka and Trachilas

374 complexes. Our data overlap with those of previous studies and display a similar range in SiO_2-K_2O (Francalanci and Zellmer,

375 2019 and reference therein). The samples of Polyegos are similar to the Fyriplaka and Trachilas complexes, whereas the older

376 Milos samples overlap with Kimolos and Antimilos (Fytikas et al., 1986, Francalanci et al., 2007).

377 Although some samples of Antimilos are tholeiitic, all of the Milos volcanic units belong to the calc-alkaline and medium to

378 high-K series (Figure 10B). A mafic inclusion, sample G15M0022, has high K_2O (6%), similar to sample G15M0021 (7.2

379 wt.%). Both of them were collected from the Vani Cape area (Fig. 2). The SiO_2 wt.% versus our $^{40}Ar/^{39}Ar$ ages diagram (Figure

380 11A) shows that there is a tendency of the volcanic units to become more felsic over time. In the diagram with K_2O/SiO_2

381 versus age there is no significant change (Figure 11C).

3.3 Variations of rock texture and eruption volume with ages

383 Figure 11D and E show the variations of crystallinity and vesicularity of the studied samples versus the $^{40}Ar/^{39}Ar$ ages. There

384 is lack of geochemical and petrological data of the pumice deposit of the Profitis Illias (>3.0 Ma). The other old pumiceous

385 pyroclastic unit, Filakopi (~2.66 Ma) volcano, has low crystallinity (<10%) and high vesicularity (10-100%) based on the data

386 of Stewart (2003). Before 1.48 Ma, the crystallinity of the Milos volcanic units is relatively high (10-40%) and vesicularity

387 varies between 1-10%. After 1.48 Ma, the lava unit of the Halepa dome and the young pumiceous unit of Trachilas and

388 Fyriplaka complexes (<1.0 Ma) have low crystallinity (<10%), and the high vesicularity (10-100%) . The volcanic complex

389 of Milos was largely (~85% by volume) constructed before ~1.48 Ma (Figure 11A). During 1.48 Ma-present, only a small

390 volume (~15%) of rhyolitic magma was added from different eruption vents.

4 Discussion

392 In this section, our $^{40}Ar/^{39}Ar$ results are compared with previously published geochronological data, and subsequently used to

393 refine the stratigraphy of the Milos VF. In the last part, we will discuss the temporal variations in major elements and the

394 volumetric volcanic output rate of the Milos VF.

4.1 Comparison with the previous geochronological studies on the Milos VF

396 K-Ar ages may show undesirable and unresolvable scatter due to various problems: (1) in accurate determination of radiogenic

397 argon due to either incorporation of excess argon or incomplete degassing of argon during the experiments; (2) inclusion of

398 cumulate or wall rock phenocrysts in bulk analyses; (3) disturbance of a variety of geological processes such as slow cooling,

399 thermal reheating; (4) unrecognized heterogeneities due to separate measurements of potassium and argon content by different

400 methods; (5) requirement of relatively large quantities (milligrams) of pure sample (e.g. Lee, 2015). In addition to these

401 methodological issues, in the case of Milos we observe that hydrothermal alteration caused substantial kaolinitisation, in

402 particular the felsic volcanic samples, that most likely has affected the K-Ar systematics. Some of these issues are also valid

403 for the $^{40}Ar/^{39}Ar$ method, however, the K-Ar method does not allow testing if ages are compromised.

^{40}Ar/^{39}Ar ages only need isotopes of argon to be measured from a single aliquot of sample with the same equipment that can eliminate some of the problems with sample inhomogeneity. Furthermore, step heating and multiple single fusion experiments can shed light on sample inhomogeneity due to partial alteration effects. The high sensitivity of modern noble gas mass spectrometers for ^{40}Ar/^{39}Ar measurements results in very small sample amounts needed for analysis, that can yield more information on the thermal or alteration histories than larger samples. Moreover, other argon isotopes (^{36}Ar, ^{37}Ar and ^{38}Ar) can be used to infer some information about the chemical compositions (i.e. Ca and Cl) of samples. A high-resolution laser incremental heating method of ^{40}Ar/^{39}Ar dating allows us to resolve the admixture of phenocryst-hosted inherited ^{40}Ar in the final temperature steps of the incremental step heating experiments. More than half of our ^{40}Ar/^{39}Ar ages derived for this study are based on this method. All incremental step heating experiments are reproducible, except for the sample G15M0017 which gave the oldest age. The total fusion experiments of this study gave at least five times smaller analytical uncertainty (1SE on average ≤0.01 Ma) than the previous studies using conventional K-Ar (Angelier et al., 1977; Fytikas et al., 1976, 1986; Matsuda et al., 1999) and SHRIMP U/Pb zircon methods (Stewart and McPhie, 2006). Fission track dating on obsidians of the Milos VF produced two ages (Bigazzi and Radi, 1981; Arias et al., 2006) which seems to overlap with the K-Ar and ^{40}Ar/^{39}Ar ages, but with larger uncertainty. U/Pb zircon ages could indicate the timing of zircon formation at high temperature (>1000 °C) in magma chambers significantly prior to volcanic eruption (e.g. Flowers et al., 2005). On the other hand, the lower closure temperature of K-rich minerals (<700 °C) makes the K-Ar and ^{40}Ar/^{39}Ar ages better suited to determine the timing of extrusion of volcanic products (e.g. Grove and Harrison, 1996; Cassata and Renne, 2013).

The MSWD value, as a measure of the scatter of the individual step ages, is based on the error enveloping around the data point. The decrease in error will automatically cause an increase in MSWD (e.g. York, 1968; Wendt and Carl, 1991). The MSWD values reported in this study are relatively high. In part this is caused by the fact that modern multi-collector mass spectrometers used for ^{40}Ar/^{39}Ar dating can measure the isotope ratios very precisely, which in turn would increase theMSWD. It will be more valuable and challenging to find a plateau or isochron age which meets the MSWD criteria (<2.5) by modern multi-collector ^{40}Ar/^{39}Ar dating than by K-Ar or ^{40}Ar/^{39}Ar dating using a single detector instrument (e.g. Mark et al., 2009).

Potential drawbacks of the ^{40}Ar/^{39}Ar method are its dependence on neutron irradiation causing the production of interfering argon isotopes that need to be corrected for. The uncertainty in ages of standards that are required to quantify the neutron flux also need to be incorporated in the final ages as are uncertainties related to decay constants (supplementary material II). Finally, recoil can occur during irradiation. Minerals such as biotite can be prone to recoil, yielding slightly older ages (e.g. Hora et al., 2010).

Figure 13 compares previous published K-Ar, U/Pb zircon and fission track ages from the same volcanic units with the new ^{40}Ar/^{39}Ar data of this study. In general, there is a good agreement, however, six ages out of twenty-three differ significantly from previous studies that will be discussed below.

The obsidian fission track ages (Bigazzi and Radi, 1981; Arias et al., 2006) for the Dhemeneghaki volcano are 0.25 My younger than the K-Ar ages (1.84 Ma, Angelier et al., 1977) and the ^{40}Ar/^{39}Ar age of this study (1.825 Ma, G15M0032B). The good agreement between the K-Ar and ^{40}Ar/^{39}Ar ages suggests that the fission track ages record another, lower temperature event, than the K-Ar and ^{40}Ar/^{39}Ar ages. In addition, the larger uncertainty of fission track ages (>0.05 Ma) also overlaps with the ^{40}Ar/^{39}Ar age at 2-sigma. We assume that the ^{40}Ar/^{39}Ar age is the correct extrusion age for the obsidian of the Dhemeneghaki volcano.

Angelier et al. (1977) reported one dacite sample in the northwest of Milos with an age of 1.71 Ma (Angelier_3, location 3 on Figure 3 of Angelier et al., 1977). Argon loss could result in these ages (Angelier_3-5 in Figure 13) being younger than our ^{40}Ar/^{39}Ar groundmass ages of 1.97 ± 0.01 Ma (dacite sample G15M0021 and -22).

The amphibole of sample G15M0004 of the Adamas dacitic lava dome, located ~1 km north of rhyolitic Bombarda volcano, gave an inverse isochron age of 1.95 Ma ± 0.45 Ma. This age overlaps with the K-Ar age for the Adamas lava dome of 2.03 ± 0.06 Ma (dacite M 66) of Fytikas et al. (1986). The large analytical uncertainty of our sample G15M0004 is caused by a

447 combination of low $^{40}Ar^*$ yields and clustering of data points that define the inverse isochron showing excess argon was

448 identified by the $^{40}Ar/^{39}Ar$ method ($^{40}Ar/^{36}Ar$ 319.51 ± 14.70), whereas the presence of excess argon cannot be tested by the

449 K-Ar technique, implying that the Fytikas et al. (1986) might be slightly old.

450 The Korakia andesite has an age of 1.59 ± 0.25 Ma (M 103, Fytikas et al., 1986) and was deposited in a submarine-subaerial

451 environment on top of the Sarakiniko Formation that was dated based on paleomagnetic polarity in combination with a K-Ar

452 age (1.80-1.85 Ma, Stewart and McPhie, 2003 and reference therein). The much older $^{40}Ar/^{39}Ar$ groundmass age (2.68 ± 0.01

453 Ma) of Korakia andesite sample G15M0029 is unreliable and it could indicate the emplacement age of the Kalogeros

454 cryptodome (2.70 ± 0.04 Ma, Stewart and McPhie, 2006) or represents a geological meaningless age with only 23-27% of the

455 total ^{39}Ar released in the "plateau". In this case, the K-Ar age of 1.59 ± 0.25 Ma is considered as the likely eruption age for the

456 Korakia andesite although its argon loss or excess Ar component is unknown.

457 We obtained $^{40}Ar/^{39}Ar$ ages of 3.41-4.10 Ma and 3.06 ± 0.02 Ma, respectively, from the groundmasses of dacite samples

458 G15M0017 and G15M0015 in the southwest of Milos (Figure 2 and 14B). Both of these samples are derived from the coherent

459 dacite facies of the rhyolitic Profitis Illias volcano based on the Figure 11 of Stewart and McPhie (2006). Sample G15M0015

460 yielded much higher radiogenic ^{40}Ar (41.77%) than that of sample G15M0017 (<10% of $^{40}Ar^*$), and the rhyolite sample M

461 164 from Fytikas et al. (1986) (23.5% of $^{40}Ar^*$) gave an estimate the eruptive age of 3.08 ± 0.08 Ma to the Profitis Illias

462 volcano which is much younger than that given by our sample G15M0017 (Figure 13). Therefore, we considered our $^{40}Ar/^{39}Ar$

463 ages of 3.06 ± 0.02 Ma is the best estimate of the emplacement age of the coherent dacite facies of Profitis Illias volcano.

464 A basaltic andesite dyke near Kleftiko on the south-western coast of Milos has a K-Ar age of 3.50 ± 0.14 Ma which only gave

465 13.9% of $^{40}Ar^*$ (Fytikas et al. 1986). This age is significantly older than the eruptive ages of Profitis Illias volcano which they

466 intrude (Stewart, 2003). Although containing relatively low $^{40}Ar^*$ (16.87%), our $^{40}Ar/^{39}Ar$ age of 2.66 ± 0.01 Ma with 67.27%

467 of $^{40}Ar^*$ from the groundmass of basaltic andesitic sample G15M0016 of the dyke near Kleftiko is probably an accurate

468 intrusion age.

469 **4.2 The published ages of other volcanic units**

470 Unfortunately, we were not able to date all key volcanic units of the Milos VF. This has three reasons (1) we did not collect

471 samples from all units; (2) some of the collected samples were not fresh enough after inspection of thin sections; and (3) some

472 of the $^{40}Ar/^{39}Ar$ data indicates that the K-Ar decay system was disturbed. Therefore, we include published age information to

473 establish a complete high-resolution geochronology for the Milos VF.

474 The published volcanic units that we include are the Profitis Illias volcano (3.08 ± 0.08 Ma with 23.5 (%), Fytikas et al., 1986),

475 the Mavro Vouni lava dome (2.50 ± 0.09 Ma with 55.2 $^{40}Ar^*$ (%), Anglier et al., 1977) in the south-western part of Milos, the

476 Bombarda volcano (1.71 ± 0.05 Ma with 24.3 $^{40}Ar^*$ (%), Fytikas et al., 1986), the Plakes volcano (0.97 ± 0.06 Ma with 10.2

477 $^{40}Ar^*$ (%), Fytikas et al., 1986, and 0.8-1.2 Ma with 5.4-11.9 $^{40}Ar^*$ (%) Matsuda et al. 1999). Scoria deposits that Stewart and

478 McPhie (2006) attributed to an andesitic scoria cone between Milos and Kimolos were produced insubmarine, and maybe

479 occasionally above sea level. No age data for this deposit has been published so far. However, the stratigraphic position of

480 this scoria deposit is between MIL 365 (2.66 Ma, Stewart and McPhie, 2006) and M103 (1.59 Ma, Fytikas et al., 1986), which

481 is shown in Figure 10 of Stewart and McPhie (2006). Therefore, this scoria cone was likely active in the north-eastern part of

482 the Milos VF between 2.6 and 1.6 Ma.

483 Fytikas et al. (1986) also analysed a pumice from the Sarakiniko deposits eastward of Adamas (1.85 ± 0.10 Ma with 13.6 $^{40}Ar^*$

484 (%), Fytikas et al., 1986) (Fig. 2). This unit is a reworked pyroclastic sediment of the Adamas lava dome (Rinaldi and Venuti,

485 2003). Therefore, the K-Ar age from the Sarakiniko unit is not considered as an eruption age in this study. We did not sample

486 the neighbouring islands of the Milos VF and also did not attempt to date the products of the recent phase of phreatic activity

487 that Traineau and Dalabakis (1989) obtained ^{14}C ages of 200 BC and 200 AD.

4.3 Implications for the stratigraphy of the Milos VF

4.3.1. Start of volcanism in the Milos VF.

Figures 13 and 14 summarize our stratigraphic interpretation of the Milos VF based on our new $^{40}Ar/^{39}Ar$ ages in combination with previously published stratigraphic, biostratigraphic, fission track, ^{14}C, K-Ar and U-Pb ages. We did not consider the Matsuda et al. (1999) data as the fission-track ages seem to be offset to other dating techniques ages obtained from the same deposits (see section 4.1 above). The exact start of volcanism in the Milos VF is still unclear since these older deposits are strongly hydrothermally altered. Van Hinsbergen et al. (2004) reported five ash layers in the Pliocene sedimentary rocks of southern Milos, ranging between 4.5-3.7 Ma in age, based on biostratigraphy, magnetostratigraphy and astronomical dating. In a slightly wider circle around Milos island, the 6.943 ± 0.005 Ma a1-tephra event recorded in several locations on nearby Crete (Rivera et al., 2011), shows that explosive volcanism along the Aegean arc, possibly on Milos, already occurred during the Messinian. These ash beds cannot be traced to currently exposed centres in the Milos VF and could conceivably be related to volcanic centres further north (Antiparos and Patmos), which were active during this time interval (Vougioukalakis et al., 2019).

Biostratigraphy shows that the youngest layer with dateable fossils (bio-event, the last common occurrence of *Sphenolithus* spp., Van Hinsbergen et al., 2004) in the Neogene sedimentary rocks is 3.61 Ma old (GTS2020, Raffi et al., 2020). The diatomite Unit II from Calvo et al. (2012) on top of the oldest volcaniclastic deposit from the north-eastern coast of Milos is constrained within 2.83-3.19 Ma. These data suggest that the oldest products must be older than 2.83 Ma and younger than 3.61 Ma. Our oldest $^{40}Ar/^{39}Ar$ ages of this study displayed a wide range of 3.41-4.10 Ma that are probably not correct due to alteration of the samples. Alteration might induce Ar loss and that would imply that the age is even older than 3.4-4.1 Ma. The age of 3.50 ± 0.14 Ma given by Fytikas et al. (1986) for an andesitic pillow lava or dyke has been discussed above and probably belongs to a series of basaltic andesite intrusions in the younger dacitic-rhyolitic deposits of Profitis Illias (~ 3.08 Ma, Fytikas et al., 1986), and therefore the 3.5 Ma age is probably not correct (e.g. Stewart, 2003). Fytikas et al. (1986) measured one sample from Kimolos (Figure 2 and 3) with an age of 3.34 Ma. Furthermore, Ferrara et al. (1980) reported an age of 3.15 Ma for a lithic clast derived from the Petalia intrusion in the Kastro volcaniclastics of Polyegos. If we assume that this reported age is a cooling age, volcanism in the Milos VF must have started before 3.15 Ma. Although age constraints for the start of volcanism on Milos both from the Neogene sedimentary rocks and the dated volcanic samples are poor, the evidence at this stage would suggest that volcanism in the Milos VF started ~3.3 Ma ago.

4.3.2. Periods with different volumetric output.

The volume estimates of the Milos VF are hampered by limited exposure of several volcanic units and unknown age relationships. Therefore, not all units can be attributed to a certain volcano. Furthermore, we also do not know how much volcanic material was lost through transport by air, sea currents and erosion. Given the large errors on these estimates, we only considered the rough difference in density between extruded magma and the calculated DRE values. The volumetric contributions of the islands Polygos, Kimolos and Antimilos are not considered here. Therefore, the discussion here only provides a first order estimate of the onshore extruded magma volume. Taken into account all these limitations, our age data and the volume estimates by Stewart and McPhie (2006) likely indicate at least three periods of different long term volumetric volcanic output rates (Q_e) throughout the Milos volcanic activity of ~3.3 - 0.0 Ma. We define a "Period" as a time interval were the Q_e is significantly different from the average output rate of the Milos VF over the last 3.3 Ma. Figure 11 shows that the Q_e can be subdivided into two slow growth periods (I and III) and one period (II) during which the Q_e was significantly larger.

The lower boundary of Period I is based on our estimate of the first volcanic units of Milos at ~3.3 Ma. These first units have been deposited in the SW of Milos between ~3.3 and 3.08 Ma (see above) that were mapped as large pumiceous deposits of the basal pyroclastic series by Fytikas et al. (1986) and the felsic pumice cone/crypto dome facies by Stewart and

McPhie (2006). These deposits have a minimum thickness of 120m. The estimates of the DRE volume and Q_e of these earliest volcanic deposits are hampered by the lack of precise age information, the high degree of alteration and structural complexities. Therefore, we only calculated the Q_e of Period I since 3.08 Ma from which the eruption products are mainly dacitic-rhyolitic in composition (Table 5, Fig 11), and the first products that can be reliable dated are cryptodomes (3.06 Ma, sample G15M0015) and dikes (2.66 Ma, sample G15M0016) into the older basal pyroclastic series of Fytikas et al. (1986) or the units of Profitis Illias volcano of Stewart and McPhie (2006, 3.08 Ma) in the SW of Milos. This was followed by the formation of the submarine Fylakopi pumice cone volcano at 2.66 Ma (Stewart and McPhie, 2006) and Kalogeros cryptodome at 2.62 Ma (sample G15M0006) in the north-eastern part of Milos. These two pumice cone volcanoes contributed 3-11 km^3 DRE in volume to the Milos VF. The last two volcanic activities of Period I occurred in the SW (Mavro Vauni, 2.50 Ma, Angelier et al., 1977) and west of Milos (Mavros Kavos, 2.36 Ma, this study), respectively, which produced two high-aspect-ratio andesitic-dacitic lava domes with a total volume of 1-3 km^3 DRE (Stewart and McPhie, 2006). During Period I, which lasted ~ 1 Myr, the estimated Q_e is $0.9 \pm 0.5 \times 10^{-5}$ km^3.yr^{-1}.

The change from Period I to II is based on the sharp increase in Q_e of Figure 11 at 2.13 Ma. During this period the Q_e ($3.0 \pm 1.7 \times 10^{-5}$ km^3.yr^{-1}) increased by a factor of ~3 compared to ~~the~~ Period I and III. Period II starts with the extrusions of the dacitic-rhyolitic Triades lava dome in the north-west and dacitic Adamas lava dome in the north-east of Milos and is followed by the rhyolitic Dhemeneghaki pumice cone/cryptodome and the Bombardo volcano in the north-east of Milos. For the Bombarda centre a large age range is reported in the literature (1.71-2.15 Ma, Fig. 13B). We ~~were~~ not ~~successful to~~ date samples from the Bombarda centre, but Rinaldi and Campos Venuti (2003) reported that an age of 1.71 Ma is the best approximation based on other stratigraphic information. For the Dhemeneghaki centre, we obtained a ^{40}Ar/^{39}Ar age of 1.825 $\pm$ 0.002 Ma from obsidian. The Triades, Adamas, Dhemeneghaki and Bombarda centres all developed in ~~a~~ submarine setting, as the intercalated sediments from the northern coast of Milos show (Calvo et al., 2012; see Fig. 14). The last two volcanic expressions in Period II consists of two submarine-to-subaerial lava dome extrusions, Kantaro (1.59 Ma, Fytikas et al., 1987) and Korakia (1.48 Ma, this study) in the north-west and north-east of Milos, respectively. The products of these two centres are andesitic-dacitic in composition. All volcanic centres of Period II produced 8-30 km^3 DRE in volume for the Milos VF. Each dome of Period II has a massive core and flow banded rind surrounded by an in-situ autobreccia zone (Stewart and McPhie, 2006).

Period III starts with a time interval of 0.4 Ma with no eruptions and has a very low Q_e of $0.25 \pm 0.05 \times 10^{-5}$ km^3.yr^{-1}. The boundary between Period II and III can be placed at the last eruption of Period II, at the start of the first eruption in the low output interval, or halfway in between. The difference between those options is not significant, given the large uncertainties of the volume estimates (Fig. 12), and therefore we have decided to start Period III directly after the last eruption of the high Q_e of Period II. The composition of nearly all Period III volcanic products is rhyolitic, an exception is the dacitic Plakes lava dome (Fig. 12). The Plakes lava dome is probably the last volcano erupting at ~0.97 Ma (Fytikas et al., 1987) in a submarine environment in the north of Milos, whereas the other lava dome in Period III, Halepa, produced rhyolitic lavas in a subaerial setting in the south (Stewart and McPhie, 2006). The Halepa and Plakes domes contributed 1-3 km^3 DRE in volume to the Milos VF and were followed by a 0.3 Ma interval with no or limited volcanic eruptions. Two subaerial pumice cone volcanoes with biotite bearing rhyolites were constructed during the last 0.6 Ma: Trachilias and Fyriplaka complexes. The Trachilas complex was active for approximately 300 kyr (0.63-0.32 Ma) in the northern part of Milos. The evolution of this complex starts with phreatic eruptions which became less explosive over time (Fytikas et al., 1986). During the last eruption (0.317 $\pm$ 0.004 Ma) of the Trachilas complex rhyolitic pumices filled up the crater area and did breach the northern tuff cone walls. The Trachilas complex only added a small volume (1-2 km^3 DRE) of material to the Milos VF. The Kalamos lava dome was also extruded in the south of Milos (Fig. 2) contemporaneously with the Trachilas complex.

The youngest volcanic activity of Milos (0.11 Ma-present), is characterized by subaerial eruptions of biotite phyric rhyolite from the Fyriplaka complex in the south of Milos, and was studied in detail by Campos Venuti and Rossi (1996). This

complex is constructed on a paleosol that developed in a phreatic deposit ("Green Lahar", Fytikas et al., 1986) or lies directly on the metamorphic basement. Campos Venuti and Rossi (1996) indicated that the stratigraphic order is: Fyriplaka and Gheraki tuff rings, Fyriplaka lava flow, composed tuff cone of Tsigrado-Provatas. The tuff ring of Fyriplaka was divided into three members, with on top the deposits of the Tsigrado tuff cone. The total estimated volume of volcanic material is 0.18 km^3 DRE. The boundary between the Fyriplaka and Tsigrado tuff cones is characterized by a marked erosive unconformity. The composition of these young volcanic products is very constant (Fig. 10-11), this was also noted by Fytikas et al (1986) and Campos Venuti and Rossi (1996). The products from Fyriplaka and Tsigrado cones are covered with a paleosol rich in archaeological remains and a phreatic deposit consisting largely of greenschist metamorphic fragments. According to Campos Venuti and Rossi (1996), the Fyriplaka cone was quickly built by phreatic and phreatomagmatic eruptions, as there are no paleosols observed between the different units. However, our data do suggest a large range in ages between 0.11 and 0.06 Ma. Fytikas et al. (1986) also reported a range between 0.14 and 0.09 Ma. These ages are inconsistent with the "Green Lahar" age of 27 kyrs (Principe et al., 2002), suggesting that the "Green Lahar" deposit consists of many different phreatic eruption layers that were formed during a time interval of more than 0.4 Ma, as the Kalamos lava is underlain by a green phreatic eruption breccia (Campos Venuti and Rossi 1996). We, therefore, conclude that phreatic eruptions occurred for more than 400 kyr, predominately in the eastern part of Milos until historical times (200 BC – 200 AD, Traineau and Dalabakis, 1989).

4.3.3. Temporal evolution of the magma plumbing system of the Milos VF.

Figure 11 shows several of the temporal petrographic and major-element variations during the evolution of the Milos VF. The chemistry of the magmas did not change significantly between the three different periods, for example, the K$_2$O/SiO$_2$ ratio is constant (0.05 ±0.02) with one exception, sample G15M0021 collected near Cape Vani which is altered by hydrothermal processes (e.g. Alfieris et al. 2013). The volcanic units of Period III are dominantly rhyolitic in composition, whereas during Period I and II the compositions of volcanic units range between basaltic-andesite to rhyolite. The crystallinity of the volcanic products is low (<10 vol.%) during Period III because most of these products are pumiceous. Although there is also a large number of pumiceous units of low crystallinity produced by Profitis Illias and Fylakopi volcanoes during Period I (Stewart and McPhie, 2006), the crystallinity of the other products of Period I and most of Period II units are much higher (20-40 vol.%) than that of Period III. In addition, we observed that the volcanic products of Period II have the lowest vesicularity (<10 vol.%), compared to the highly variable vesicularity of Period I (1-50 vol.%) and the high value for Period III (10-100 vol.%). These observations are consistent with the type of volcanic structures. Period I and III contain large explosive pumice cone volcanoes, whereas Period II is dominated by effusive dome extrusions. The extrusion of crystal-rich, outgassed and thus viscous residual magmas in large volumes during Period II is similar to the description for the effusive volcanism of the Methana VF (Popa et al., 2020). Popa et al. (2020) suggested that the critical factor controlling the effusive-explosive transitions of Methana is the crystallinity of the erupted material based on their petrological data. The crystallinity has a higher influence on the bulk viscosity of magma than the other factors (e.g. water content and composition; Popa et al., 2020). A higher crystallinity results in a slower ascent velocity of magma and enhances the formation of permeable pathways in the conduit for the gas, which promotes the outgassing of the magmas and leads to effusive behaviour. Lower crystallinity (<30 vol.%) of the magmas results in explosive eruptions and has the opposite effect on outgassing, which causes high vesicularity of the eruption products.

Popa et al. (2020) showed that different magma plumbing systems are responsible for the explosive (crystal-poor) and effusive (crystal-rich) eruptions of Methana (Popa et al., 2020, their Fig. 13). For the effusive lava domes of Period II, the composition mainly ranges from basaltic-andesitic to dacitic, and the petrological observations of the dacite sample G15M0019 and -20 of the Kantaro dome show the presence of olivine-clinopyroxene-orthopyroxene cumulates and amphibole-biotite reaction rims (supplementary material I). The andesite of the Korakia dome (G15M0029) has a groundmass of acicular plagioclase and plagioclase phenocrysts with sieve textures. These petrological observations suggest large scale magma mixing between felsic and more mafic magma, consistent with the hybridized magmas of the effusive events on Methana (e.g. Popa et al., 2020). The

pumiceous units of the explosive volcanoes on Milos during Period I and III could be caused by mafic magmas that intrudes a magma reservoir filled with felsic magma. This is consistent with the suggestion of Fytikas et al. (1986) that the main location of feeding magma for the Milos VF is in the lower part of the crust from Pliocene to Pleistocene ($\approx$Period I).

It is noteworthy that the value of the Q_e (0.2-4.7$\times$10^{-5} km^3.yr^{-1}) for the Milos VF is at least 2-3 orders lower than the average for rhyolitic systems (4.0$\times$10^{-3} km^3.yr^{-1}) and the mean for continental arcs ($\sim$70$\times$10^{-3} km^3.yr^{-1}) with a range of 8$\times$10^{-6} – 9$\times$10^{-2} km^3.yr^{-1} (White et al., 2006). Milos overlaps with the lowest Q_e values of the study of White et al. (2006). For the magma supply rate underneath the Milos VF, although no data are available for the ratio between intruded magma in the crust below Milos and extruded volcanics (I:E), White et al. (2006) argue that a ratio of 5:1 is probably a realistic estimate for most volcanic centres and that this ratio can be higher in volcanic centres constructed on continental crust. This would result in a magma supply rate from the mantle beneath the Milos VF in the order of 0.1-3.3$\times$10^{-4} km^3.yr^{-1}. Compared with other SAVA volcanic centres, Druitt et al. (2019) reported a long-term average magma supply rate of approximately 1$\times$10^{-3} km^3.yr^{-1} beneath the Kameni islands of Santorini, which is comparable to that of the Milos. Besides the case of Santorini VF, no other information on the long-term average magma supply rate of other volcanic centres of the SAVA is available to our knowledge. Given that the island of Milos is approximately 15 km long (W-E), this results in a magma production rate over the last $\sim$3.34 Ma of approximately 0.7-22 km^3.km^{-1}.Myr^{-1}. Although this magma production rate per km arc length is the onshore estimate for the Milos VF, it is still significant lower than for oceanic arcs: 157-220 km^3.Myr^{-1}.km^{-1} (Jicha and Jagoutz, 2015). For continental arcs the long-term magma production rate is more difficult to establish because magmatism is cyclic, and short periods (5-20 Ma) of intense magmatism ("flare ups") with 85 km^3.km^{-1}.Myr^{-1} are alternating with periods of 25-50 Ma of low magma production rate of 20 km^3.km^{-1}.Myr^{-1} (e.g. Jicha and Jagoutz, 2015). The periods of low magma production overlap with the magma production rates beneath the Milos VF over the past $\sim$3.34 Ma.

5 Conclusion

This study reports twenty-one new ^{40}Ar/^{39}Ar ages and major element data for 10 volcanic units of the Milos Volcanic Field. In combination with previously published age data, geochemistry and facies analysis the following points can be made.

(1) The exact age of the start of volcanism in the Milos VF is still unclear due to the high degree of alteration of the oldest deposits. The best estimate is based on our new ^{40}Ar/^{39}Ar ages, published K-Ar data and nannofossil biozones is between 3.5 and 3.15 Ma.

(2) Based on the long-term volumetric volcanic output rate, the volcanic history of the Milos VF can be divided into two slow growth periods, Period I ($\sim$3.3-2.36 Ma) and III (1.48 Ma-present), and one relatively fast growth period, Period II (2.36-1.48 Ma).

(3) Period I and III are dominated by low crystallinity, highly vesicular pumice deposits, whereas Period II is characterised by dominantly dome extrusions with low versicular, high crystallinity products.

(4) Large scale magma mixing between felsic and more mafic magma in the upper crust underneath Milos probably result in the high crystallinity of the effusively eruptive units of Period II. During Period I and III, the pumiceous units of the explosive volcanoes on Milos could be caused by mafic magma from deep that intrudes a magma reservoir filled with felsic magma. The evolution of the Milos VF volcanic rocks changed over time in composition from basaltic-andesite-rhyolite volcanism to mainly rhyolite. The long term volumetric volcanic output rate of Milos is 0.2-4.7$\times$10^{-5} km^3.yr^{-1}, 2-3 orders of magnitude lower than the average for rhyolitic systems and continental arcs.

Acknowledgement

We would like to thank Roel van Elsas with the assistance of rock crushing and mineral separation. Kiki Dings helped with the XRF bead preparation and measurements. Lara Borst and Onno Postma assisted with the ^{40}Ar/^{39}Ar dating. We acknowledge the Greek Institute of Geology and Mineral Exploration (IGME) for permission to conduct fieldwork on Milos. Xiaolong Zhou would like to acknowledge a grant no. 201506400055 from the China Scholarship Council (CSC). The ^{40}Ar/^{39}Ar facility of the VU is covered by NWO grant 834.09.004. This research benefitted from funding from the European Research Council under the European Union's Seventh Framework Programme (FP7/2007-2013)/ERC grant agreement n° 319209. A previous version of this manuscript greatly benefitted from a very detailed and constructive review by Dr. J. McPhie. A second review by Dr J. McPhie and Dr. J-F. Wotzlaw helped to clarify the interpretation of the geochronology of Milos. We thank Drs. J. Nadden, J. Miles and S Tapster for pointing out mistakes in our figures.

References

Alfieris, D., Voudouris, P. and Spry, P. G.: Shallow submarine epithermal Pb-Zn-Cu-Au-Ag-Te mineralization on western Milos Island, Aegean Volcanic Arc, Greece: Mineralogical, geological and geochemical constraints, Ore Geol. Rev., 53, 159–180, doi:10.1016/j.oregeorev.2013.01.007, 2013.

Angelier, J., Cantagrel, J.-M. and Vilminot, J.-C.: Neotectonique cassante et volcanisme plio-quaternaire dans l'arc egeen interne; l'ile de Milos (Grece), Bull. la Société Géologique Fr., 7(1), 119–124, 1977.

Arias, A., Oddone, M., Bigazzi, G., Di Muro, A., Principe, C. and Norelli, P.: New data for the characterization of Milos obsidians, J. Radioanal. Nucl. Chem., 268(2), 371–386, doi:10.1007/s10967-006-0183-9, 2006.

Berger, G. W. and York, D.: Geothermometry from 40Ar39Ar dating experiments, Geochim. Cosmochim. Acta, 45(6), 795–811, doi:10.1016/0016-7037(81)90109-5, 1981.

Bigazzi, G. and Radi, G.: Datazione con le tracce di fissione per l'identificazione della provenienza dei manufatti di ossidiana, Riv. di Sci. Preist., 36/1–2, 223–250, 1981.

Calvo, J. P., Triantaphyllou, M. V., Regueiro, M. and Stamatakis, M. G.: Alternating diatomaceous and volcaniclastic deposits in Milos Island, Greece. A contribution to the upper Pliocene-lower Pleistocene stratigraphy of the Aegean Sea, Palaeogeogr. Palaeoclimatol. Palaeoecol., 321–322, 24–40, doi:10.1016/j.palaeo.2012.01.013, 2012.

Campos Venuti, M. and Rossi, P. L.: Depositional facies in the Fyriplaka rhyolitic tuff ring, Milos Island (Cyclades, Greece), Acta Vulcanol., 8, 173–192, 1996.

Cassata, W. S. and Renne, P. R.: Systematic variations of argon diffusion in feldspars and implications for thermochronometry, Geochim. Cosmochim. Acta, 112, 251–287, doi:10.1016/j.gca.2013.02.030, 2013.

Cole, P. D., Calder, E. S., Sparks, R. S. J., Clarke, A. B., Druitt, T. H., Young, S. R., Herd, R. A., Harford, C. L. and Norton, G. E.: Deposits from dome-collapse and fountain-collapse pyroclastic flows at Soufrière Hills Volcano, Montserrat, Geol. Soc. London, Mem., 21(1), 231–262, 2002.

Crosweller, H. S., Arora, B., Brown, S. K., Cottrell, E., Deligne, N. I., Guerrero, N. O., Hobbs, L., Kiyosugi, K., Loughlin, S. C. and Lowndes, J.: Global database on large magnitude explosive volcanic eruptions (LaMEVE), J. Appl. Volcanol., 1(1), 4, 2012.

Druitt, T. H., Edwards, L., Mellors, R. M., Pyle, D. M., Sparks, R. S. J., Lanphere, M., Davies, M. and Barreirio, B.: Santorini Volcano, Geol. Soc. Mem., 19 [online] Available from: http://pubs.er.usgs.gov/publication/70094778, 1999.

Druitt, T. H., Pyle, D. M. and Mather, T. A.: Santorini Volcano and its Plumbing System, Elements, 15(3), 177–184, doi:10.2138/gselements.15.3.177, 2019.

Duermeijer, C. E., Nyst, M., Meijer, P. T., Langereis, C. G. and Spakman, W.: Neogene evolution of the Aegean arc: Paleomagnetic and geodetic evidence for a rapid and young rotation phase, Earth Planet. Sci. Lett., 176(3–4), 509–525, doi:10.1016/S0012-821X(00)00023-6, 2000.

Ferrara, G., Fytikas, M., Giuliani, O. and Marinelli, G.: Age of the formation of the Aegean active volcanic arc, Thera Aegean world II, 2, 37–41, 1980.

Flowers, R. M., Bowring, S. A., Tulloch, A. J. and Klepeis, K. A.: Tempo of burial and exhumation within the deep roots of a magmatic arc, Fiordland, New Zealand, Geology, 33(1), 17–20, doi:10.1130/G21010.1, 2005.

Francalanci, L. and Zellmer, G. F.: Magma Genesis at the South Aegean Volcanic Arc, Elements, 15(3), 165–170, doi:10.2138/gselements.15.3.165, 2019.

Francalanci, L., Vougioukalakis, G. E., Fytikas, M., Beccaluva, L., Bianchini, G. and Wilson, M.: Petrology and volcanology of Kimolos and Polyegos volcanoes within the context of the South Aegean arc, Greece, Spec. Pap. Soc. Am., 418, 33, 2007.

Frey, H. M., Lange, R. A., Hall, C. M. and Delgado-Granados, H.: Magma eruption rates constrained by 40Ar/39Ar chronology and GIS for the Ceboruco-San Pedro volcanic field, western Mexico, Bull. Geol. Soc. Am., 116(3–4), 259–276,

710 doi:10.1130/B25321.1, 2004.

711 Fytikas, M., Giuliani, O., Innocenti, F., Marinelli, G. and Mazzuoli, R.: Geochronological data on recent magmatism of the

712 Aegean Sea, Tectonophysics, 31(1–2), T29–T34, doi:10.1016/0040-1951(76)90161-X, 1976.

713 Fytikas, M., 1977. Geology and Geothermics of Milos Island. Thesis, Thessaloniki Uni- versity, 228 pp. (in Greek with

714 English summary).

715 Fytikas, M., Innocenti, F., Kolios, N., Manetti, P., Mazzuoli, R., Poli, G., Rita, F. and Villari, L.: Volcanology and petrology

716 of volcanic products from the island of Milos and neighbouring islets, J. Volcanol. Geotherm. Res., 28(3–4), 297–317,

717 doi:10.1016/0377-0273(86)90028-4, 1986.

718 Fytikas, M.: Updating of the geological and geothermal research on Milos island, Geothermics, 18(4), 485–496,

719 doi:10.1016/0375-6505(89)90051-5, 1989.

720 Grasemann, B., Huet, B., Schneider, D. A., Rice, A. H. N., Lemonnier, N. and Tschegg, C.: Miocene postorogenic extension

721 of the Eocene synorogenic imbricated Hellenic subduction channel: New constraints from Milos (Cyclades, Greece), Bull.

722 Geol. Soc. Am., 130(1–2), 238–262, doi:10.1130/B31731.1, 2018.

723 Grove, M. and Harrison, T. M.: 40Ar* diffusion in Fe-rich biotite, Am. Mineral., 81(7–8), 940–951, 1996.

724 Hayes, G. P., Moore, G. L., Portner, D. E., Hearne, M., Flamme, H., Furtney, M. and Smoczyk, G. M.: Slab2, a

725 comprehensive subduction zone geometry model, Science (80-.)., 362(6410), 58–61, doi:10.1126/science.aat4723, 2018.

726 Hildreth, W. and Lanphere, M. A.: Potassium-argon geochronology of a basalt-andesite-dacite arc system: The Mount

727 Adams volcanic field, Cascade Range of southern Washington, Geol. Soc. Am. Bull., 106(11), 1413–1429, 1994.

728 Hildreth, W., Fierstein, J. and Lanphere, M.: Eruptive history and geochronology of the Mount Baker volcanic field,

729 Washington, Geol. Soc. Am. Bull., 115(6), 729–764, 2003a.

730 Hildreth, W., Lanphere, M. A. and Fierstein, J.: Geochronology and eruptive history of the Katmai volcanic cluster, Alaska

731 Peninsula, Earth Planet. Sci. Lett., 214(1–2), 93–114, doi:10.1016/S0012-821X(03)00321-2, 2003b.

732 Van Hinsbergen, D. J. J., Snel, E., Garstman, S. A., Marunţeanu, M., Langereis, C. G., Wortel, M. J. R. and Meulenkamp, J.

733 E.: Vertical motions in the Aegean volcanic arc: Evidence for rapid subsidence preceding volcanic activity on Milos and

734 Aegina, Mar. Geol., 209(1–4), 329–345, doi:10.1016/j.margeo.2004.06.006, 2004.

735 Hora, J. M., Singer, B. S., Jicha, B. R., Beard, B. L., Johnson, C. M., de Silva, S. and Salisbury, M.: Volcanic biotite-

736 sanidine 40Ar/39Ar age discordances reflect Ar partitioning and pre-eruption closure in biotite, Geology, 38(10), 923–926,

737 doi:10.1130/G31064.1, 2010.

738 IJlst, L.: A laboratory overflow-centrifuge for heavy liquid mineral separation, Am. Mineral., 58, 1088–1093, 1973.

739 Jicha, B. R. and Jagoutz, O.: Magma production rates for intraoceanic arcs, Elements, 11(2), 105–112,

740 doi:10.2113/gselements.11.2.105, 2015.

741 Kilias, S. P., Naden, J., Cheliotis, I., Shepherd, T. J., Constandinidou, H., Crossing, J. and Simos, I.: Epithermal gold

742 mineralisation in the active Aegen volcanic arc: The Profitis Ilias deposits, Milos Island, Greece, Miner. Depos., 36(1), 32–

743 44, doi:10.1007/s001260050284, 2001.

744 Koppers, A. A. P.: ArArCALC-software for 40Ar/39Ar age calculations, Comput. Geosci., 28(5), 605–619,

745 doi:10.1016/S0098-3004(01)00095-4, 2002.

746 Kornprobst, J., Kienast, J.-R. and Vilminot, J.-C.: The high-pressure assemblages at Milos, Greece, Contrib. to Mineral.

747 Petrol., 69(1), 49–63, doi:10.1007/bf00375193, 1979.

748 Kuiper, K. F., Deino, A., Hilgen, F. J., Krijgsman, W., Renne, P. R. and Wijbrans, J. R.: Synchronizing Rock Clocks of

749 Earth History, Science (80-.)., 320(5875), 500–504, doi:10.1126/science.1154339, 2008.

750 Lee, J. K. W.: Ar–Ar and K–Ar Dating BT - Encyclopedia of Scientific Dating Methods, edited by W. Jack Rink and J. W.

751 Thompson, pp. 58–73, Springer Netherlands, Dordrecht., 2015.

752 Lee, J. Y., Marti, K., Severinghaus, J. P., Kawamura, K., Yoo, H. S., Lee, J. B. and Kim, J. S.: A redetermination of the

isotopic abundances of atmospheric Ar, Geochim. Cosmochim. Acta, 70(17), 4507–4512, doi:10.1016/j.gca.2006.06.1563, 2006.

Mark, D. F., Barfod, D., Stuart, F. M. and Imlach, J.: The ARGUS multicollector noble gas mass spectrometer: Performance for 40Ar/39Ar geochronology, Geochemistry, Geophys. Geosystems, 10(10), 1–9, doi:10.1029/2009GC002643, 2009.

Matsuda, J., Senoh, K., Maruoka, T., Sato, H. and Mitropoulos, P.: K-Ar ages of the Aegean the volcanic rocks and arc-trench system their implication for the arc-trench system, Geochem. J., 33, 369–377, 1999.

McKenzie, D.: Active tectonics of the Alpine—Himalayan belt: the Aegean Sea and surrounding regions, Geophys. J. Int., 55(1), 217–254, 1978.

Meulenkamp, J. E., Wortel, M. J. R., van Wamel, W. A., Spakman, W. and Hoogerduyn Strating, E.: On the Hellenic subduction zone and the geodynamic evolution of Crete since the late Middle Miocene, Tectonophysics, 146(1–4), 203–215, doi:10.1016/0040-1951(88)90091-1, 1988.

Min, K., Mundil, R., Renne, P. R. and Ludwig, K. R.: A test for systematic errors in 40Ar/39Ar geochronology, Geochim. Cosmochim. Acta, 64(1), 73–98, 2000.

Nicholls, I. A.: Santorini volcano, greece - tectonic and petrochemical relationships with volcanics of the Aegean region, Tectonophysics, 11(5), 377–385, doi:10.1016/0040-1951(71)90026-6, 1971.

Pe-Piper, G. and Piper, D. J. W.: The South Aegean active volcanic arc: relationships between magmatism and tectonics, Dev. Volcanol., 7(C), 113–133, doi:10.1016/S1871-644X(05)80034-8, 2005.

Pe-Piper, G. and Piper, D. J. W.: Neogene backarc volcanism of the Aegean: New insights into the relationship between magmatism and tectonics, Geol. Soc. Am. Spec. Pap., 418(02), 17–31, doi:10.1130/2007.2418(02), 2007.

Pe-Piper, G. and Piper, D. J. W.: The effect of changing regional tectonics on an arc volcano: Methana, Greece, J. Volcanol. Geotherm. Res., 260, 146–163, doi:10.1016/j.jvolgeores.2013.05.011, 2013.

Raffi, I., Wade, B. S., Pälike, H., Beu, A. G., Cooper, R., Crundwell, M. P., Krijgsman, W., Moore, T., Raine, I. and Sardella, R.: The Neogene Period, in Geologic Time Scale 2020, pp. 1141–1215, Elsevier., 2020.

Rinaldi, M. and Venuti, M. C.: The submarine eruption of the Bombarda volcano, Milos Island, Cyclades, Greece, Bull. Volcanol., 65(4), 282–293, doi:10.1007/s00445-002-0260-z, 2003.

Rivera, T. A., Storey, M., Zeeden, C., Hilgen, F. J. and Kuiper, K.: A refined astronomically calibrated 40Ar/39Ar age for Fish Canyon sanidine, Earth Planet. Sci. Lett., 311(3–4), 420–426, doi:10.1016/j.epsl.2011.09.017, 2011.

Rontogianni, S., Konstantinou, N. S., Melis, C. P. and Evangelidis: Slab stress field in the Hellenic subduction zone as inferred from intermediate-depth earthquakes, Earth, Planets Sp., 63(2), 139–144, doi:10.5047/eps.2010.11.011, 2011.

Schaen, A., Jicha, B., Hodges, K., Vermeesch, P., Stelten, M., Mercer, C., Phillips, D., Rivera, T., Jourdan, F., Matchan, E., Hemming, S., Morgan, L., Kelley, S., Cassata, W., Heizler, M., Vasconcelos, P., Benowitz, J., Koppers, A., Mark, D., Niespolo, E., Sprain, C., Hames, W., Kuiper, K., Turrin, B., Renne, P., Ross, J., Nomade, S., Guillou, H., Webb, L., Cohen, B., Calvert, A., Joyce, N., Ganerød, M., Wijbrans, J., Ishizuka, O., He, H., Ramirez, A., Pfänder, J., Lopez-Martínez, M., Qiu, H. and Singer, B.: Interpreting and reporting 40Ar/39Ar geochronologic data, GSA Bull., doi:10.1130/B35560.1, 2020.

Singer, B. S., Thompson, R. A., Dungan, M. A., Feeley, T. C., Nelson, S. T., Pickens, J. C., Brown, L. L., Wulff, A. W., Davidson, J. P. and Metzger, J.: Volcanism and erosion during the past 930 k.y. at the Tatara–San Pedro complex, Chilean Andes, Geol. Soc. Am. Bull., 109(2), 127–142, doi:10.1130/0016-7606(1997)109<0127:VAEDTP>2.3.CO;2, 1997.

Sonder, R. A.: Zur Geologie and Petrographie der Inselgruppe yon Milos, Zeitschr. Volc., 8, 11–231, 1924.

Spakman, W., Wortel, M. J. R. and Vlaar, N. J.: The Hellenic Subduction Zone: A tomographic image and its geodynamic implications, Geophys. Res. Lett., 15(1), 60–63, doi:10.1029/GL015i001p00060, 1988.

Stewart, A. L.: Volcanic Facies Architecture and Evolution of Milos, Greece, University of Tasmania., 2003.

Stewart, A. L. and McPhie, J.: Internal structure and emplacement of an Upper Pliocene dacite cryptodome, Milos Island, Greece, J. Volcanol. Geotherm. Res., 124(1–2), 129–148, doi:10.1016/S0377-0273(03)00074-X, 2003.

796 Stewart, A. L. and McPhie, J.: An Upper Pliocene coarse pumice breccia generated by a shallow submarine explosive

797 eruption, Milos, Greece, Bull. Volcanol., 66(1), 15–28, doi:10.1007/s00445-003-0292-z, 2004.

798 Stewart, A. L. and McPhie, J.: Facies architecture and Late Pliocene – Pleistocene evolution of a felsic volcanic island,

799 Milos, Greece, Bull. Volcanol., 68(7–8), 703–726, doi:10.1007/s00445-005-0045-2, 2006.

800 Traineau, H. and Dalabakis, P.: Mise en evidence d'une eruption phreatique historique sur l'ile de Milos (Grece), CR Acad

801 Sci Paris, 1–38, 1989.

802 Vougioukalakis, G. E., Satow, C. G. and Druitt, T. H.: Volcanism of the South Aegean volcanic arc, Elements, 15(3), 159–

803 164, 2019.

804 Wendt, I. and Carl, C.: The statistical distribution of the mean squared weighted deviation, Chem. Geol. Isot. Geosci. Sect.,

805 86(4), 275–285, doi:10.1016/0168-9622(91)90010-T, 1991.

806 White, S. M., Crisp, J. A. and Spera, F. J.: Long-term volumetric eruption rates and magma budgets, Geochemistry,

807 Geophys. Geosystems, 7(3), 262–266, doi:10.1029/2005GC001002, 2006.

808 York, D.: Least squares fitting of a straight line with correlated errors, Earth Planet. Sci. Lett., 5(C), 320–324,

809 doi:10.1016/s0012-821x(68)80059-7, 1968.

810

Table 1. Published eruption ages of stratigraphic units of the island of Milos

Stratigraphy	Sample	Mineral	Location	Petrology	K₂O (wt.%)	Age (Ma)	± 1σ
Unit IV	[1]Angelier_1	Unknown	Fyriplaka	Rhyolite	-	-	-
Unit III	[1]Angelier_2	Unknown	Halepa	Rhyolite	2.44	0.95	0.06
Unit II	[1]Angelier_3	Unknown	Triades	Dacite	1.47	1.71	0.08
	[1]Angelier_4	Unknown	Kleftico	Andesite	1.77	2.33	0.09
	[1]Angelier_5	Unknown	Kleftico	Andesite	1.45	2.50	0.09
Unit I	[1]Angelier_6	Unknown	Adamas	Rhyolite	2.90	2.15	0.08
	[1]Angelier_7	Unknown	Dhemeneghaki	Rhyolite	2.75	1.84	0.08
Phreatic activity	[5]Gif-7358&7359	Carbonized wood	Agia Kiriaki	Lahar deposits	-	200 BC-200 AD	
CFT	[2]M196	Unknown	Fyriplaka	Rhyolite	2.9	0.09	0.02
	[2]M194	Unknown	Fyriplaka	Rhyolite	2.85	0.14	0.03
	[2]M168	Unknown	Trachilas	Rhyolite	3.91	0.37	0.09
	[2]M-48	Biotite	NW of Filiplaka	Rhyolite	6.41	0.48	0.05
PSLD	[3]MI-1	Lava	Plakes	Dacite	2.07	0.80	0.10
	[2]M-OB1	Groundmass	N of Dhemenegaki	Obsidian	2.53	0.88	0.18
	[2]M27	Unknown	Plakes	Dacite	1.87	0.97	0.06
	[3]MI-4	Lava	Plakes	Dacite	2.32	1.20	0.10
	[4]MIL130	Zircon	Triades	Dacite	-	1.44	0.08
	[2]M-OB2	Groundmass	Bombarda	Obsidian	2.73	1.47	0.05
	[6]Fission track1	Groundmass	Adamas	Obsidian	-	1.54	0.18
	[6]Fission track2	Groundmass	Bombarda	Obsidian	-	1.57	0.15
	[7]Fission track3	Groundmass	Bombarda-Adamas	Obsidian	-	1.57	0.12
	[2]M103	Unknown	near Pollonia	Andesite	1.87	1.59	0.25
	[7]Fission track3	Groundmass	Dhemeneghaki	Obsidian	-	1.60	0.06
	[2]M146	Unknown	1km NW of Adamas	Rhyolite	3.09	1.71	0.05
	[2]M110	Unknown	Sarakiniko	Dacite	2.57	1.85	0.10
CDLF	[2]M1	Unknown	Aghios, near Triades	Rhyolite	3.32	2.04	0.09
	[2]M66	Unknown	~1 km NW of Adamas	Dacite	2.61	2.03	0.06
	[4]MIL243	Zircon	Triades	Dacite	-	2.18	0.09
	[2]M156	Unknown	Angathia, near Triades	Dacite	2.84	2.38	0.10
BPS	[4]MIL365	Zircon	Filakopi	Rhyolite	-	2.66	0.07
	[4]MIL343	Zircon	Kalogeros cryptodome	Dacite	-	2.70	0.04
	[2]M164	Unknown	Kleftico	Rhyolite	2.84	3.08	0.08
	[2]M163	Unknown	Kleftico	Andesite	1.18	3.50	0.14

Published ages from 1=Angelier et al. (1977), 2=Fytikas et al. (1976, 1986), 3=Matsuda et al. (1999), 4=Stewart and McPhie (2006), 5=Trainau and Dalabakis (1989), 6=Bigazzi and Radi (1981), Arias et al. (2006). Angelier et al. (1977) do not provide sample names, only numbers for the sample locations. Here the location is given after "Angelier_" (Angelier et al. 1977, their Fig. 3). Abbreviations: BPS=Basal pyroclastic series; CDLF=Complex of domes and lava flows; PSLD=Pyroclastic series and lava domes; CTF=Complexes of Trachilas and Fyriplaka. See more details in Fig. 4.

Table 2. Incremental heating $^{40}Ar/^{39}Ar$ results of the Milos volcanic field.

Volcanic Unit	Sample-ID	Irr-ID	Latitude	Age ± 1σ (Ma)	MSWD	$^{39}Ar_K$ (%)	n/ntotal	$^{40}Ar^*$ (%)	K/Ca ± 1σ	Inverse isochron age (Ma)	$^{40}Ar/^{36}Ar$ ± 1σ	MSWD
Fyriplaka Complex	G15M0008[B]	VU110-Z22a	36.6729 N 24.4670 E	0.05 ± 0.01	0.04	16.24	3/15	1.20	60.9 ± 10.6	0.05 ± 0.10	298.08 ± 8.77	0.08
		VU110-Z22b		**0.062 ± 0.003**	0.91	71.81	8/11	2.69	57.3 ± 8.4	0.06 ± 0.02	299.39 ± 3.66	1.09
		Combined (Z22)		0.061 ± 0.004	0.82	41.37	11/26	2.29	58.0 ± 6.3	0.07 ± 0.01	296.78 ± 1.78	0.83
	G15M0012[B]	VU110-Z24a	36.6795 N 24.4828 E	0.05 ± 0.01	3.09	38.89	3/11	2.89	40.0 ± 6.0	0.14 ± 0.03	285.98 ± 4.76	0.07
		VU110-Z24b		0.09 ± 0.02	8.16	48.04	4/11	4.59	30.1 ± 7.1	0.09 ± 0.05	297.46 ± 10.29	12.78
		Combined(Z24)		**0.07 ± 0.01**	7.44	43.53	7/22	3.86	32.3 ± 5.0	0.09 ± 0.03	295.67 ± 7.39	9.02
	G15M0009[B]	VU110-Z23a	36.6716 N 24.4891 E	0.11 ± 0.02	1.37	18.33	4/12	1.65	45.4 ± 7.3	0.76 ± 0.30	268.52 ± 17.08	0.90
		VU110-Z23b		0.11 ± 0.03	6.77	41.05	4/11	3.13	19.4 ± 3.7	0.29 ± 0.14	285.17 ± 15.80	8.09
		Combined (Z23)		**0.11 ± 0.02**	3.50	29.50	8/21	2.39	19.7 ± 2.6	0.15 ± 0.05	295.78 ± 4.34	4.04
Trachilas Complex	G15M0007[B]	VU110-Z12a	36.7671 N 24.4124 E	0.30 ± 0.01	4.61	56.50	8/16	14.51	38.3 ± 2.4	0.28 ± 0.05	301.42 ± 9.01	5.47
		VU110-Z12b		**0.317 ± 0.004**	1.29	74.05	4/11	18.30	32.0 ± 2.5	0.31 ± 0.03	299.52 ± 6.40	2.04
		Combined (Z12)		0.31 ± 0.01	5.57	65.27	12/27	15.77	33.1 ± 1.6	0.34 ± 0.03	293.05 ± 5.50	5.84
Kontaro dome	G15M0020[G]	VU108-Z5a_5	36.7234 N 24.3952 E	1.52 ± 0.01	1.06	61.82	8/12	18.30	1.51 ± 0.05	1.49 ± 0.02	300.03 ± 0.86	0.95
		VU108-Z5b_1		1.56 ± 0.01	1.94	41.54	3/10	47.94	1.73 ± 0.06	1.58 ± 0.02	294.97 ± 3.74	2.17
		VU108-Z5b_2		1.52 ± 0.01	1.73	62.45	5/10	22.95	1.56 ± 0.08	1.53 ± 0.02	298.12 ± 0.89	2.34
		Combined (Z5)		**1.54 ± 0.01**	3.06	57.32	16/32	25.31	1.58 ± 0.04	1.55 ± 0.01	297.41 ± 0.57	2.82
	G15M0019[G]	VU108-Z6a_4	36.7211 N 24.3950 E	1.62 ± 0.01	3.80	89.75	9/11	34.28	0.91 ± 0.05	1.62 ± 0.02	297.66 ± 1.36	4.40
		VU108-Z6a_5		1.55 ± 0.01	4.50	95.41	10/12	35.26	0.88 ± 0.06	1.55 ± 0.01	298.73 ± 1.29	5.40
		VU108-Z6b_1		1.56 ± 0.01	4.05	56.64	4/10	53.19	1.02 ± 0.01	**1.48 ± 0.02**	315.46 ± 5.20	0.44
		Combined (Z6)		1.55 ± 0.01	32.15	80.97	27/45	38.78	0.93 ± 0.04	1.53 ± 0.02	300.60 ± 2.27	34.25
Dheme-neghaki volcano	G15M0032B[O]	VU108-Z18	36.7084 N 24.5324 E	**1.825 ± 0.002**	0.91	98.64	12/13	93.86	1.83 ± 0.04	1.825±0.003	301.52 ± 3.34	0.93
Triades lava dome	G15M0021[B]	VU110-Z4_2	36.7402 N 24.3397 E	**1.97 ± 0.01**	1.66	63.83	4/12	54.72	107.55 ± 20.64	1.97 ± 0.03	299.16 ± 5.36	2.56
		VU110-Z4_2b		2.01 ± 0.01	6.76	75.39	6/16	57.84	54.43 ± 8.29	2.04 ± 0.05	293.08 ± 10.44	8.15
		Combined (Z4)		1.99 ± 0.01	9.08	69.12	10/28	56.59	73.52 ± 6.46	2.00 ± 0.04	295.64 ± 7.89	10.30
Adamas lava dome	G15M0004[A]	VU108-Z10_1	36.7282 N 24.4315 E	2.99 ± 0.11	1.00	87.31	4/12	16.36	0.030 ± 0.002	7.89 ± 2.46	202.39 ± 48.47	0.01
		VU108-Z10_2		2.86 ± 0.09	1.50	86.18	7/11	17.58	0.029 ± 0.002	0.70 ± 0.29	348.91 ± 27.33	1.00
		Combined (Z10)		2.90 ± 0.07	1.31	86.74	11/23	17.13	0.029 ± 0.001	**1.95 ± 0.45**	319.51 ± 14.70	1.17
The dyke of Mavro Vouni lava dome	G15M0016[G]	VU108-Z8a	36.6668 N 24.3398 E	2.71 ± 0.02	2.31	79.64	8/12	16.57	0.24 ± 0.05	2.65 ± 0.10	299.84 ± 2.32	2.92
		VU108-Z8a_4		2.61 ± 0.03	0.93	57.41	7/12	16.86	0.12 ± 0.07	2.69 ± 0.10	296.44 ± 2.49	0.69
		VU108-Z8b_1		2.67 ± 0.01	1.50	65.57	7/11	17.25	0.11 ± 0.04	2.55 ± 0.05	301.53 ± 1.14	0.71
		Combined (Z8)		**2.66 ± 0.01**	2.51	67.27	22/35	16.87	0.14 ± 0.02	2.61 ± 0.05	300.01 ± 1.18	2.78
Korokia dome	G15M0029[G]	VU108-Z16a	36.7465 N 24.5200 E	2.67 ± 0.01	0.96	23.61	4/13	56.34	0.53 ± 0.05	2.68 ± 0.02	296.64 ± 3.18	1.25
		VU108-Z16b_1		2.69 ± 0.01	1.32	27.08	3/13	55.78	0.55 ± 0.04	2.67 ± 0.03	301.16 ± 4.72	2.13
		Combined (Z16)		2.68 ± 0.01	1.66	25.30	7/26	56.10	0.54 ± 0.03	2.67 ± 0.02	300.00 ± 2.94	1.98
Coherent dacite of Profitis Illias volcano	G15M0015[G]	VU108-Z9a	36.6629 N 24.3596 E	3.12 ± 0.02	9.07	43.07	3/12	42.73	1.31 ± 0.05	3.06 ± 0.02	304.19 ± 1.25	0.01
		VU108-Z9b_1		2.98 ± 0.02	4.53	27.00	4/14	39.35	0.98 ± 0.06	3.04 ± 0.02	293.83 ± 1.38	1.14
		Combined (Z9)		2.99 ± 0.02	5.54	22.79	6/26	41.77	1.00 ± 0.04	**3.06 ± 0.02**	292.77 ± 1.62	1.90
Coherent dacite of Profitis Illias volcano	G15M0017[G]	VU108-Z7a	36.6596 N 24.3675 E	**3.64 ± 0.08**	3.13	28.62	7/13	9.77	1.04 ± 0.02	4.14 ± 0.49	293.87 ± 4.77	3.44
		VU108-Z7a_4		**4.10 ± 0.06**	2.13	34.71	6/17	9.08	1.10 ± 0.01	4.11 ± 1.40	298.44 ± 15.51	3.24
		VU108-Z7b_1		**3.41 ± 0.05**	3.95	31.41	5/13	9.95	1.00 ± 0.03	3.68 ± 0.71	295.97 ± 7.34	7.09
		Combined (Z7)		3.63 ± 0.08	14.04	31.40	18/43	9.59	1.04 ± 0.02	2.19 ± 0.32	311.31 ± 3.60	10.19

The age in bold is considered as the best estimate of the eruptive age.

The $^{40}Ar^*$ (%) is the average radiogenic ^{40}Ar of the analyses included in the weighted mean.

The experiment was analyzed on biotite[B], obsidian[O], amphibole[A] and groundmass[G] of a sample.

The same steps were used for the calculation of isochron ages as used in the weighted mean ages.

Table 3. ^{40}Ar/^{39}Ar results of single grain fusion analyses on the Milos volcanic field.

Volcanic unit	Sample-ID	Irr-ID	Location	Age ± 1σ (Ma)	MS WD	^{39}Ar$_K$ (%)	n/ ntotal	^{40}Ar* (%)	K/Ca ± 1σ	Inverse isochron age (Ma)	^{40}Ar/^{36}Ar ± 1σ	MS WD
Fyriplaka complex	G15M0008[B]	VU110-Z22	36.6729 N 24.4670 E	0.71 ± 0.06	0.41	25.78	8/23	8.67	17.5 ± 1.8	0.64 ± 0.20	302.75 ± 12.62	0.46
	G15M0012[B]	VU110-Z24	36.6795 N 24.4828 E	1.12 ± 0.11	2.26	60.49	14/23	7.32	14.9 ± 0.8	0.26 ± 0.07	316.75 ± 19.49	2.29
	G15M0009[B]	VU110-Z23	36.6716 N 24.4891 E	0.65 ± 0.07	1.16	79.91	19/23	5.87	12.0 ± 0.5	0.28 ± 0.07	309.57 ± 16.01	1.22
Trachilas complex	G15M0007[B]	VU110-Z12	36.7671 N 24.4124 E	0.47 ± 0.05	0.75	72.65	15/22	9.09	14.8 ± 0.5	0.55 ± 0.12	293.95 ± 11.30	0.80
Kalamos lava	G15M0033[B]	VU108-Z19	36.6662 N 24.4652 E	**0.412 ± 0.004**	1.10	77.24	8/10	22.22	20.5 ± 2.7	0.39 ± 0.02	303.32 ± 3.06	0.89
Trachilas complex	G15M0034[B]	VU108-Z20	36.7550 N 24.4244 E	**0.51 ± 0.02**	0.95	56.92	6/10	3.53	13.7 ± 1.2	0.61 ± 0.08	296.45 ± 1.65	0.92
	G15M0035[B]	VU108-Z21	36.7550 N 24.4244 E	**0.63 ± 0.02**	1.26	73.43	6/9	4.87	17.7 ± 1.1	0.77 ± 0.13	294.99 ± 3.17	1.42
Halepa lava dome	G15M0013[B]	VU108-Z13	36.6716 N 24.4406 E	**1.04 ± 0.01**	1.62	82.40	9/10	26.30	*15.2 ± 0.2	1.02 ± 0.04	299.77 ± 4.06	0.00
Triades lava dome	G15M0021[B]	VU110-Z4	36.7402 N 24.3397 E	2.48 ± 0.04	1.49	87.08	4/12	36.09	13.00± 0.60	3.44 ± 0.46	228.58 ± 36.66	1.39
	G15M0022[B]	VU108-Z14	36.7402 N 24.3397 E	**2.10 ± 0.01**	1.37	100.00	10/10	36.04	*11.7 ± 0.2	2.08 ± 0.06	299.44 ± 4.63	1.59
	G15M0023[B]	VU108-Z3	36.7263 N 24.3420 E	**2.10 ± 0.01**	1.72	55.58	6/11	35.93	*76.1 ± 2.4	2.13 ± 0.06	296.12 ± 4.63	2.08
	G15M0024[B]	VU108-Z15	36.7277 N 24.3415 E	**2.13 ± 0.01**	0.46	63.67	6/10	29.74	22.5 ± 3.2	2.09 ± 0.03	300.50 ± 1.58	0.23
Mavros Kavos lava dome	G15M0025[B]	VU108-Z2	36.6876 N 24.3515 E	**2.36 ± 0.01**	0.70	84.62	9/10	37.62	43.2 ± 2.7	2.34 ± 0.04	300.57 ± 3.49	0.78
	G15M0026[B]	VU108-Z1b	36.6848 N 24.3500 E	2.35 ± 0.01	1.36	95.23	9/10	38.56	12.8 ± 2.3	**2.42 ± 0.04**	292.01 ± 2.92	0.93
Kalegeros crypto-dome	G15M0006[B]	VU108-Z11	36.7643 N 24.5157 E	2.72 ± 0.01	1.95	87.67	9/10	47.90	*28.3 ± 0.5	**2.62 ± 0.04**	310.21 ± 4.04	0.99

The age in bold is considered as the best estimate of the eruptive age.

The ^{40}Ar* (%) is the average radiogenic ^{40}Ar of the analyses included in the weighted mean.

*The K/Ca ratio is calibrated by removing the total fusion with excess ^{37}Ar (Ca) (fA>1).

[B]The experiment was analyzed on biotite of the sample.

The same steps were used for the calculation of isochron ages as used in the weighted mean ages.

Table 4. Major-element composition of volcanic samples from the Milos Volcanic Field.

Sample-ID	G15M0008	G15M0012	G15M0009	G15M0007	G15M0033	G15M0034	G15M0035	G15M0013	G15M0020	G15M0019	G15M0032B	G15M0004
Rock Types	Pumice	Pumice	Pumice	Pumice	Pumice	Pumice	Pumice	Rhyolite	-	Dacite	Obsidian	Dacite
Major elements (wt.%)												
SiO_2	76.71	75.47	76.02	76.68	76.68	76.89	78.40	72.87	-	64.26	75.57	63.56
TiO_2	0.14	0.13	0.13	0.08	0.10	0.08	0.08	0.22	-	0.56	0.20	0.57
Al_2O_3	12.96	12.77	12.91	12.60	12.86	12.64	12.93	14.11	-	16.08	13.32	16.09
Fe_2O_3	1.11	1.08	1.04	0.85	0.88	0.84	0.85	1.95	-	5.33	1.46	5.70
MnO	0.06	0.06	0.06	0.08	0.09	0.09	0.09	0.07	-	0.11	0.06	0.11
MgO	0.22	0.22	0.23	0.11	0.18	0.11	0.11	0.51	-	2.42	0.33	2.81
CaO	1.27	1.27	1.19	0.75	0.85	0.74	0.76	2.23	-	5.33	1.71	6.01
Na_2O	4.04	4.12	3.99	3.58	3.71	3.50	3.49	3.73	-	3.60	3.95	3.49
K_2O	3.22	3.15	3.41	4.74	4.46	4.85	4.95	3.43	-	1.69	3.26	1.57
P_2O_5	0.02	0.02	0.02	0.01	0.01	0.01	0.01	0.04	-	0.04	0.03	0.09
BaO	0.06	0.06	0.06	0.05	0.05	0.05	0.05	0.06	-	0.04	0.06	0.04
L.O.I.	0.16	0.35	0.16	0.17	0.14	0.33	0.06	0.13	-	0.09	0.07	0.04
Total	99.97	98.70	99.22	99.70	100.01	100.13	101.78	99.35	-	99.55	100.02	100.08

Sample-ID	G15M0021	G15M0022	G15M0023	G15M0024	G15M0025	G15M0026	G15M0006	G15M0016	G15M0029	G15M0015	G15M0017
Rock Types	Trachy-dacite	Enclave	Dacite	Rhyolite	Dacite	Dacite	Dacite	Basaltic Andesite	Dacite	Dacite	Dacite
Major elements (wt.%)											
SiO2	64.98	53.87	73.05	76.57	69.56	69.57	68.58	**55.72**	61.91	63.77	68.03
TiO2	0.35	0.60	0.29	0.23	0.42	0.43	0.40	0.66	0.79	0.64	0.58
Al2O3	16.82	19.91	14.24	11.73	15.30	16.08	15.90	18.43	17.09	16.33	15.90
Fe2O3	3.69	7.61	3.23	1.69	3.15	3.38	2.67	7.70	5.90	5.42	3.47
MnO	0.08	0.16	0.02	0.03	0.11	0.04	0.07	0.14	0.09	0.10	0.07
MgO	1.50	3.93	0.53	0.46	0.88	0.62	0.81	4.42	1.84	2.48	1.34
CaO	2.19	5.45	2.35	2.36	3.67	3.43	2.89	8.78	6.07	5.91	4.31
Na2O	2.61	1.73	3.28	2.85	3.49	3.56	4.19	2.90	3.57	3.35	3.76
K2O	7.24	6.11	3.36	2.31	2.98	2.63	3.61	1.41	2.71	1.91	2.69
P2O5	0.05	0.08	0.04	0.05	0.11	0.09	0.11	0.09	0.20	0.09	0.10
BaO	0.35	0.34	0.06	0.05	0.06	0.06	0.10	0.03	0.13	0.04	0.04
L.O.I.	0.17	0.21	0.12	0.20	0.19	0.09	0.12	0.06	0.09	0.04	0.48
Total	100.03	100.00	100.57	98.53	99.92	99.98	99.45	100.34	100.39	100.08	100.77

The classification of rock type for each sample is on the basis of field observation and SiO_2 versus K_2O plot of Le Bas et al. (1986). All iron expressed as Fe_2O_3T(otal).

Table 5. Summary of the eruption ages of the Milos volcanic field

No.	Name of volcanic centre	Age (Ma)	Reference
1	Kimlos volcano	3.34	Fytikas et al., 1986
2	Profitis Illias crypto/pumice cone	3.08	Fytikas et al., 1986
3	coherent dacite of Profitis Illias volcano	3.06	This study
4	Filakopi volcano	2.66	Stewart and McPhie, 2006
5	Kalegeros cryptodome	2.62	This study
6	Mavro Vouni lava dome	2.5	Angelier et al., 1977
7	Mavros Kavos lava dome	2.42-2.36	This study
8	Polyegos lava dome	2.34	Fytikas et al., 1986
9	Triades lava dome	2.13-2.10 and 1.97	This study
10	Adamas lava dome	2.03	Fytikas et al., 1986
11	Dhemeneghaki volcano	1.83	This study
12	Bombardo volcano	1.71	Fytikas et al., 1986
13	Korakia dome	1.59	Fytikas et al., 1986
14	Komntaro dome	1.52-1.48	This study
15	Halepa lava dome	1.04	This study
16	Plakes lava dome	0.97	Fytikas et al., 1986
17	Trachilias complex	0.63, 0.51 and 0.317	This study
18	Kalamos lava dome	0.41	This study
19	Antimilos domes	0.32	Fytikas et al., 1986
20	Fyriplaka complex	0.11 and 0.07-0.06	This study
21	Phreatic activity	200 AD-200 BC	Trainau and Dalabakis, 1989
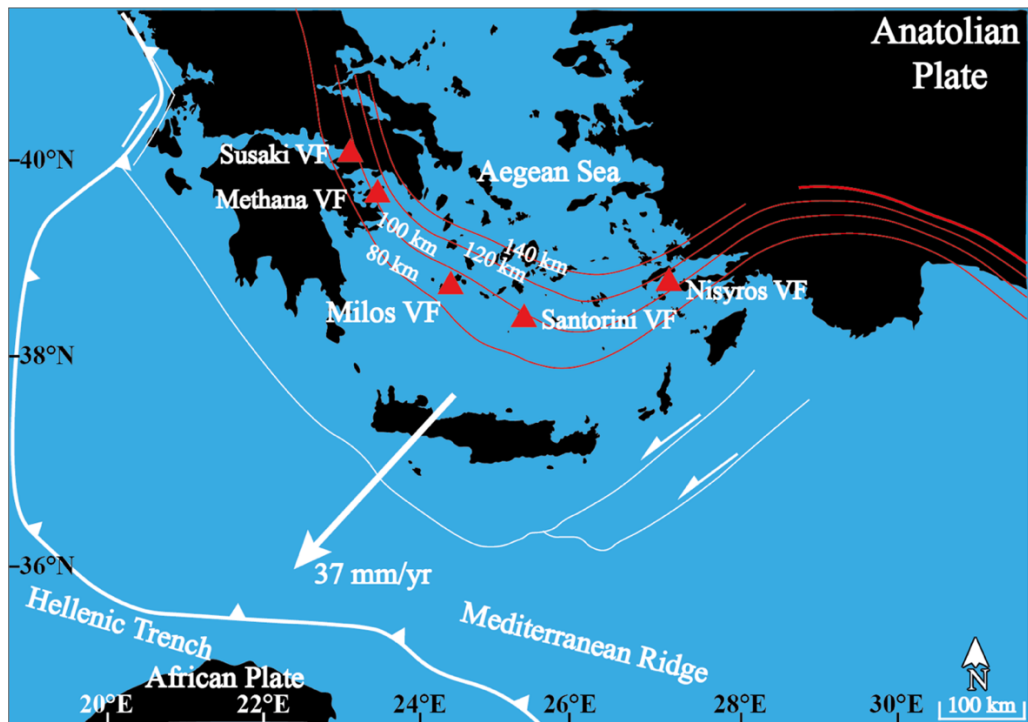
Figure 1. Map of the South Aegean Volcanic Arc (SAVA). Volcanic fields (VF) are indicated by red triangles: Susaki, Methana and Milos VFs in the western SAVA, Santorini VF in the centre and Nisyros VF in the eastern SAVA. Red contour lines show the depth to the Benioff zone (Hayes et al., 2018). White arrow represents the GPS-determined plate velocity of the Aegean microplate relative to the African plate from Doglioni et al. (2002).
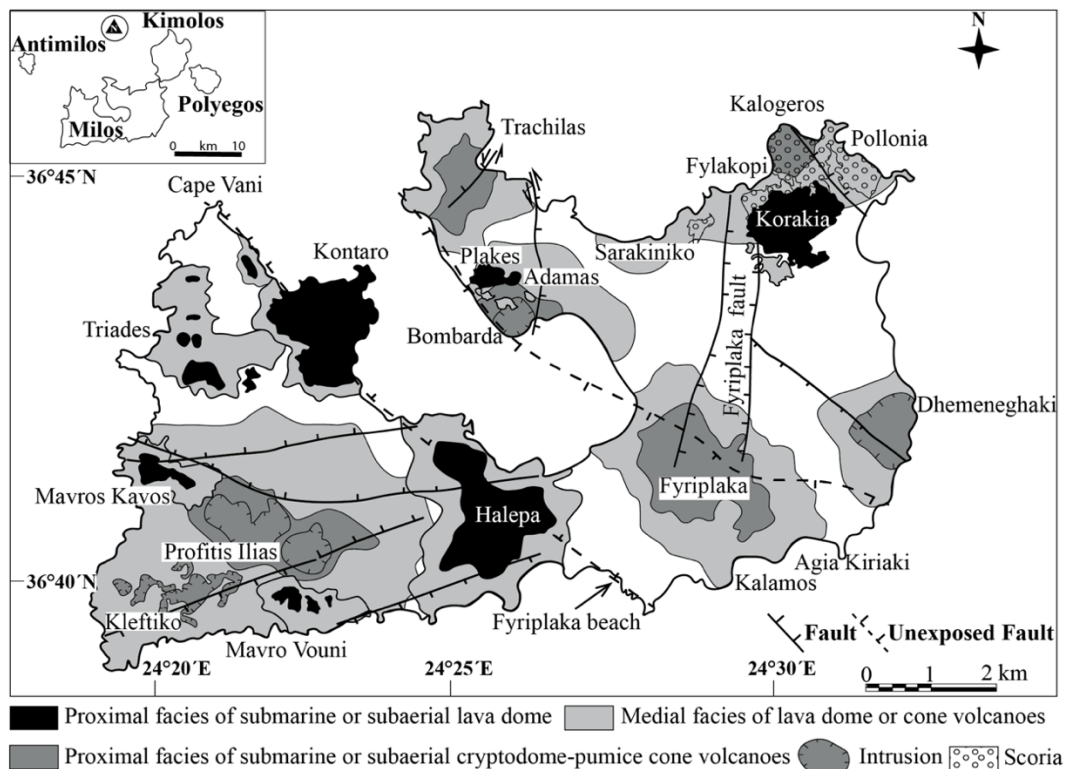
Figure 2. Distribution of the proximal and medial facies of the submarine pumice cone/crypto dome volcanoes, submarine, submarine-subaerial and subaerial domes and rhyolitic complexes (tuff cone and associated lava) of Milos, modified after Fytikas et al. (1986) and Stewart and McPhie (2006). The distal facies of Stewart and McPhie (2006) is not shown.
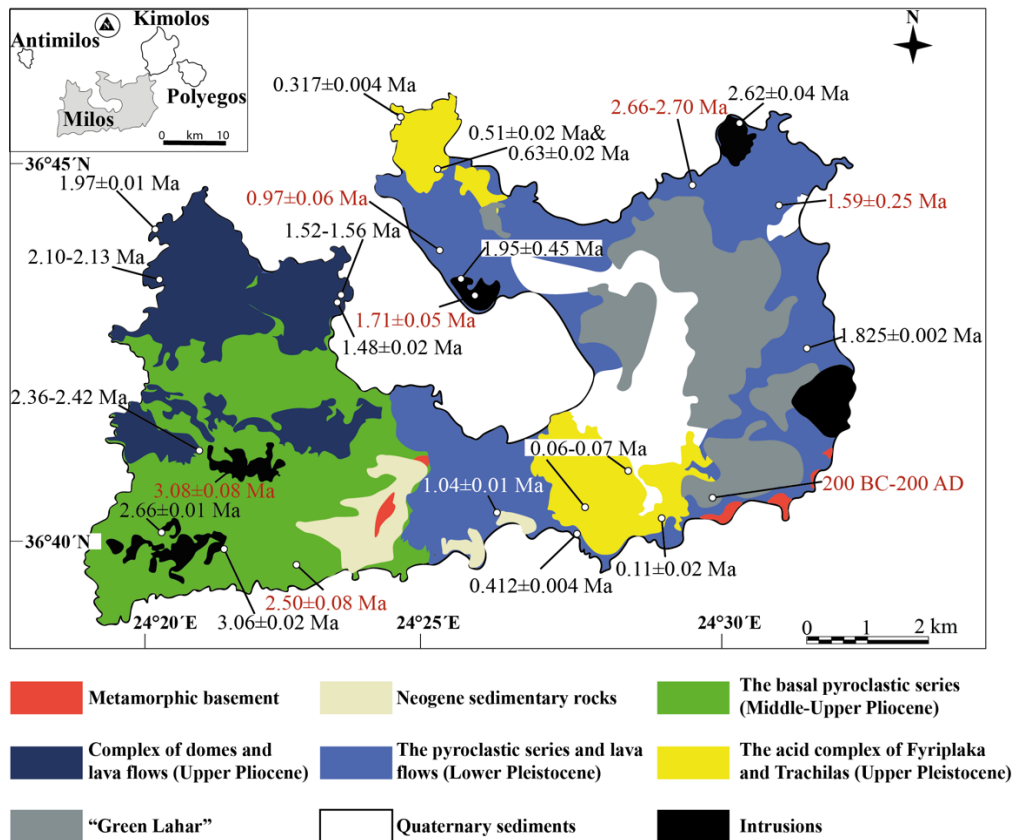
Figure 3. Simplified geological map of Milos with our ⁴⁰Ar/³⁹Ar ages and sample locations of key volcanic deposits, modified after Stewart and McPhie (2006) and Grasemann et al. (2018). The stratigraphic units of Milos are from Fytikas et al. (1986). Age data from this study are in black, published ages are shown in red (Angelier et al., 1977, Fytikas et al., 1986, Traineau and Dalabakis, 1989, and Stewart and McPhie, 2006). The "Green Lahar" (Fytikas, 1977) consists of deposits from multiple phreatic explosions and contains fragments of metamorphic, sedimentary and volcanic rocks.
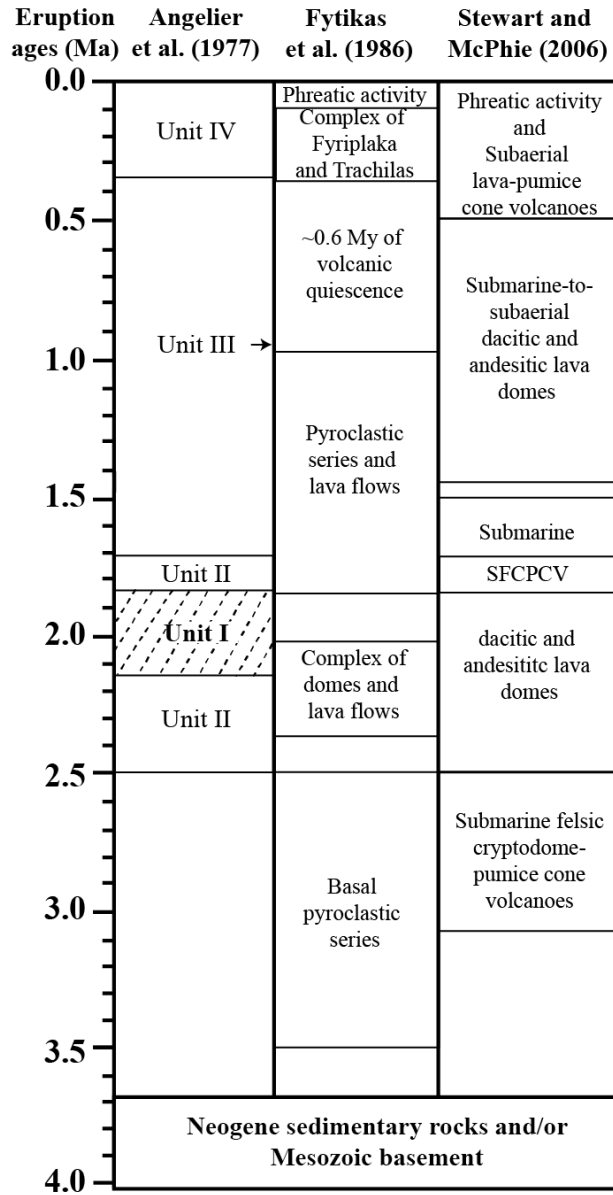
Figure 4. Previous proposed stratigraphic frameworks for Milos by Angelier et al. (1977), Fytikas et al. (1986) and Stewart and McPhie (2006). Volcanic unit II of Angelier et al. (1977) contains unit I. Stewart and McPhie (2006) described the volcanic faces of Milos mainly based on the geochronological works of Angelier et al. (1977) and Fytikas et al. (1986). Abbreviation: SFCPCV=Submarine felsic cryptodome-pumice cone volcanoes.
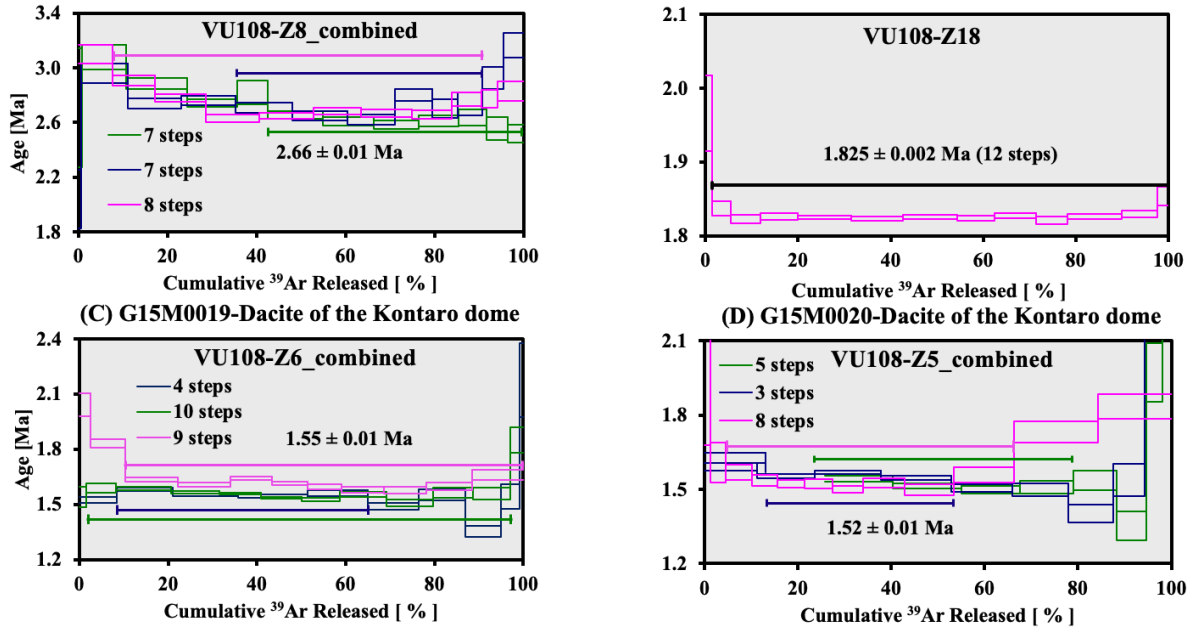
Figure 5. Groundmass $^{40}Ar/^{39}Ar$ plateau ages for samples G15M0016 (A), G15M0032B (B), G15M0019 (C) and G15M0020 (D). The Mavro Vouni dome (A), Dhemeneghaki volcano (B) and Kontaro dacitic dome (C, D) are located in respectively the south-western, north-eastern and eastern parts of Milos VF (see Fig. 2). Final age calculation is reported with 1σ errors. See the individual steps of sample G15M0016, G15M0019 and G15M0029 in supplementary material II.
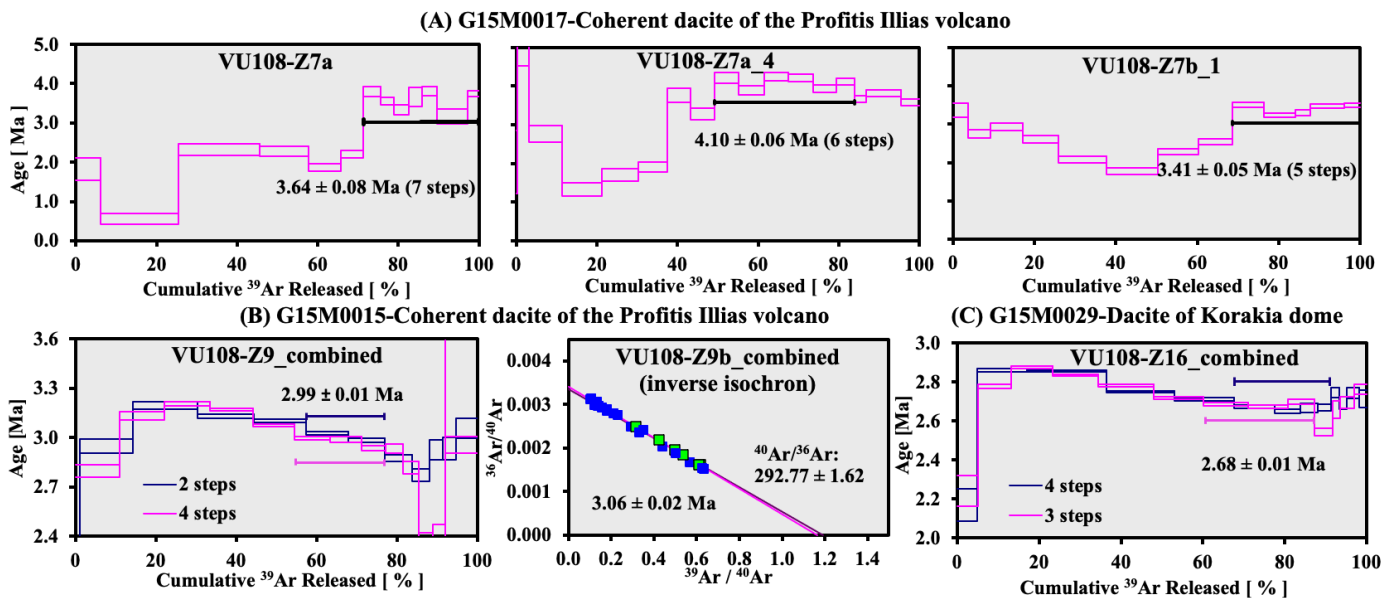
Figure 6. Groundmass $^{40}Ar/^{39}Ar$ plateau or inverse isochron ages for samples G15M0017 (A), G15M0015 (B) and G15M0029 (C). Individual steps and final age calculation are reported with 1σ errors. The Profitis Illias volcano (A, B) and dacitic Korakia dome (C) are located in the south-western and north-eastern parts of Milos VF, respectively (see Fig. 2). See the individual steps of sample G15M0015 and G15M0029 in supplementary material II.
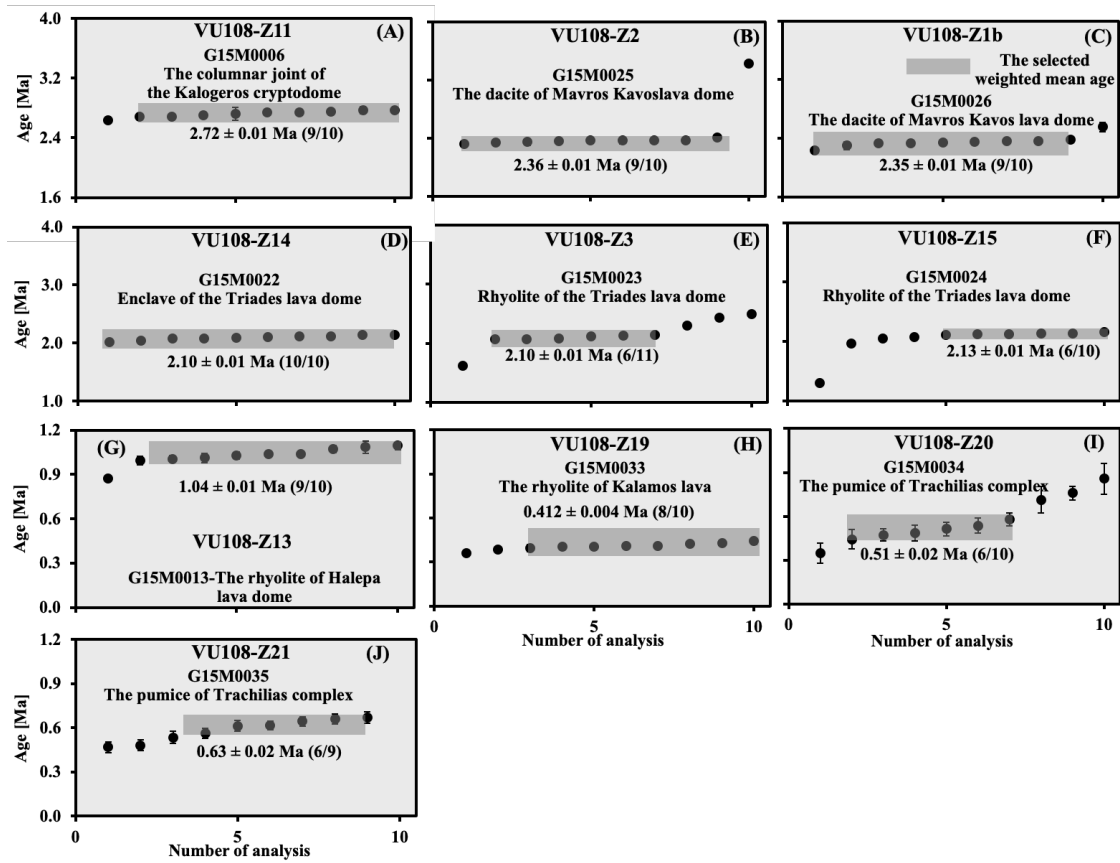
Figure 7. Biotite ^{40}Ar/^{39}Ar total fusion ages for samples G15M0006 (A) and G15M0025-26(B, C), G15M0022-24 (D-F), G15M0013 (G) and G15M0033-35 (H-J). Data outside shaded area are not included in the weighted mean. Individual steps and final age calculation are reported with 1σ errors. The Kalogeros cryptodome and Mavros Kavos lava dome are located in the north-eastern and south-western parts of Milos VF, respectively, and Triades lava dome, Halepa lava dome, Trachilias complex and the Kalamos lava are situated in the southern, northern and south-eastern parts of Milos VF, respectively (see Fig. 2).
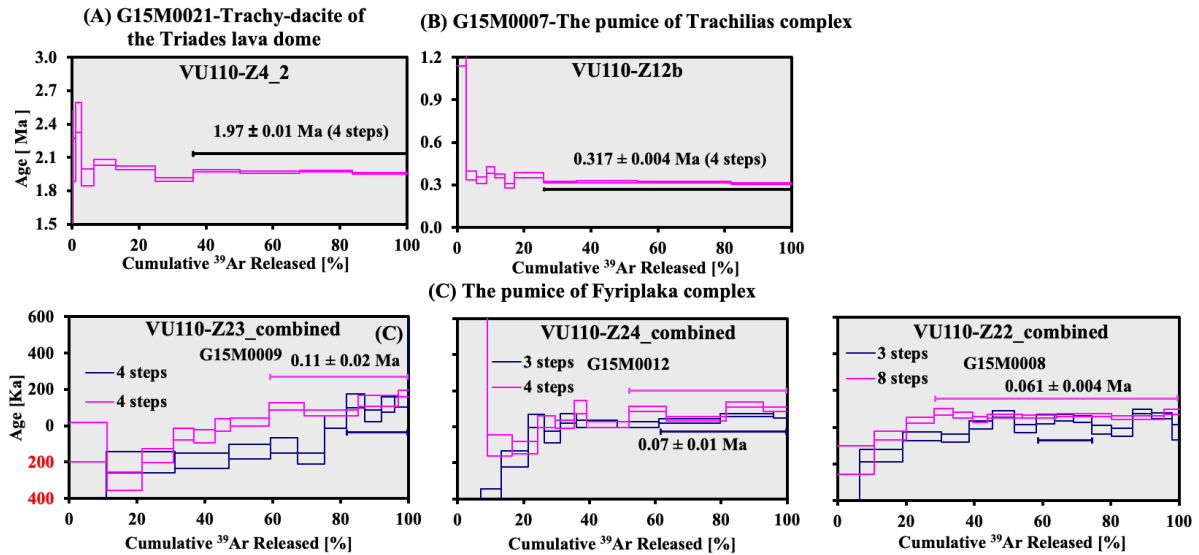
Figure 8. Biotite ^{40}Ar/^{39}Ar plateau ages for samples G15M0021 (A), G15M0007 (B), and G15M0009 (VU110-Z23_combined), G15M0012 (VU110-Z24_combined) and G15M0008 (VU110-Z22_combined) (C). The numbers in red represent negative ages. Individual steps and final age calculation are reported with 1σ errors. The Triades lava dome, Trachilias and Fyriplaka complexes are located in the north-western, northern and south-eastern parts of Milos VF, respectively (see Fig. 2). See the individual steps of sample G15M0021, G15M0007, G15M0009, G15M0012 and G15M0008 in supplementary material II.
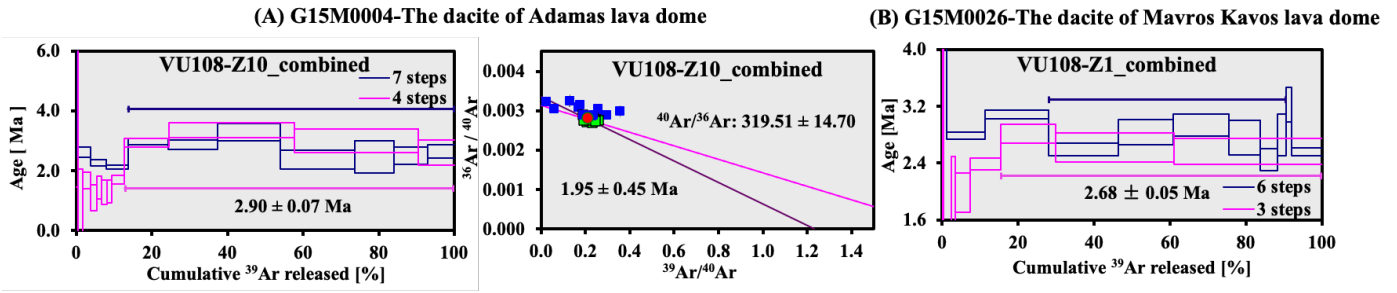
Figure 9. Amphibole $^{40}Ar/^{39}Ar$ plateau or inverse isochron ages for samples G15M0004 (A) and G15M0026 (B). Final age calculation is reported with 1σ errors. The Adamas and Mavros Kavos lava domes are located in the northern and south-western parts of Milos VF, respectively (see Fig. 2). See the individual steps of sample G15M0004 and G15M0026 in in supplementary material II.
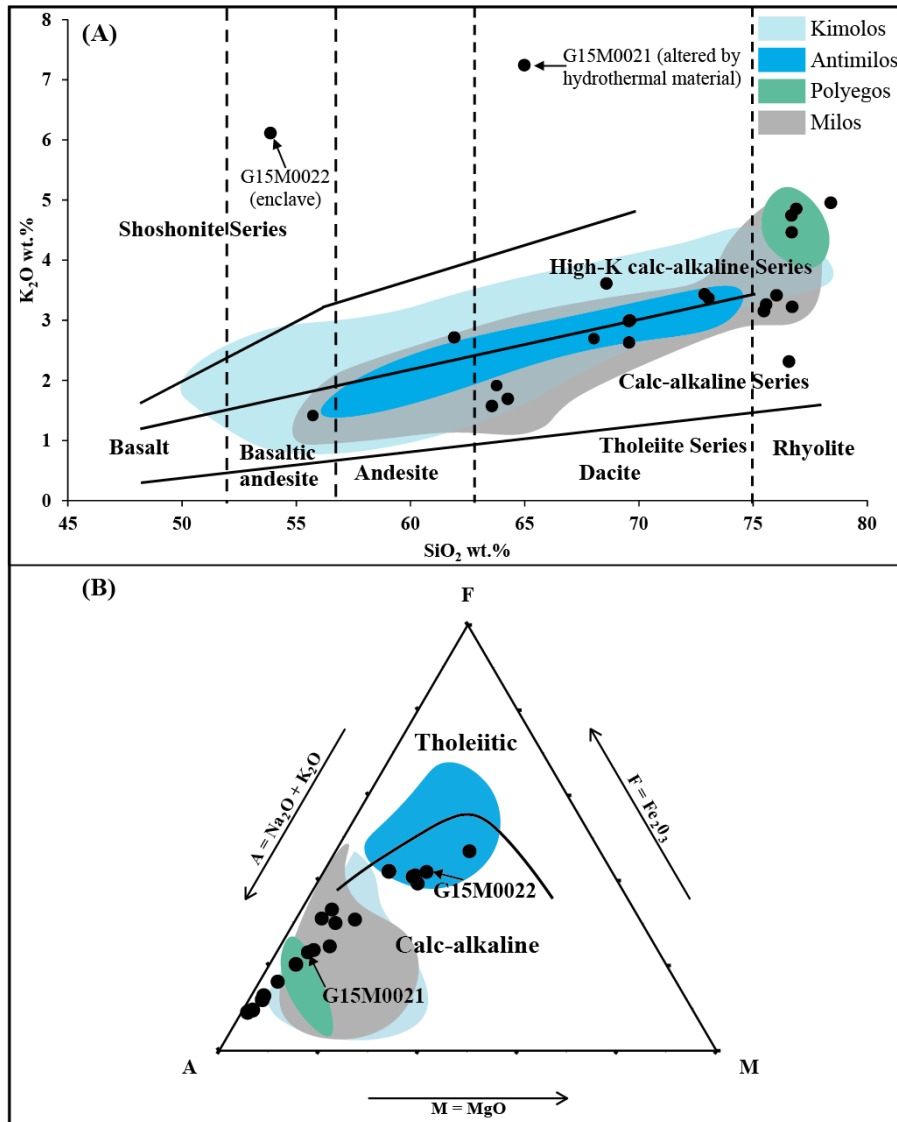
Figure 10. SiO_2 versus K_2O (A) and AFM (B) diagrams for the Milos volcanic field with data of this study as solid circles. Published data are represented by shaded fields (Francalanci and Zelmer, 2019 and reference therein). Fields for the tholeiite, calc-alkaline, high-K calc-alkaline and shoshonitic series are from Peccerillo and Taylor (1976). Vertical lines defining fields for basalt, basaltic-andesite, andesite, dacite and rhyolite are from Le Bas et al. (1986). The solid line dividing tholeiitic and calc-alkaline fields is from Irvine and Baragar (1971).
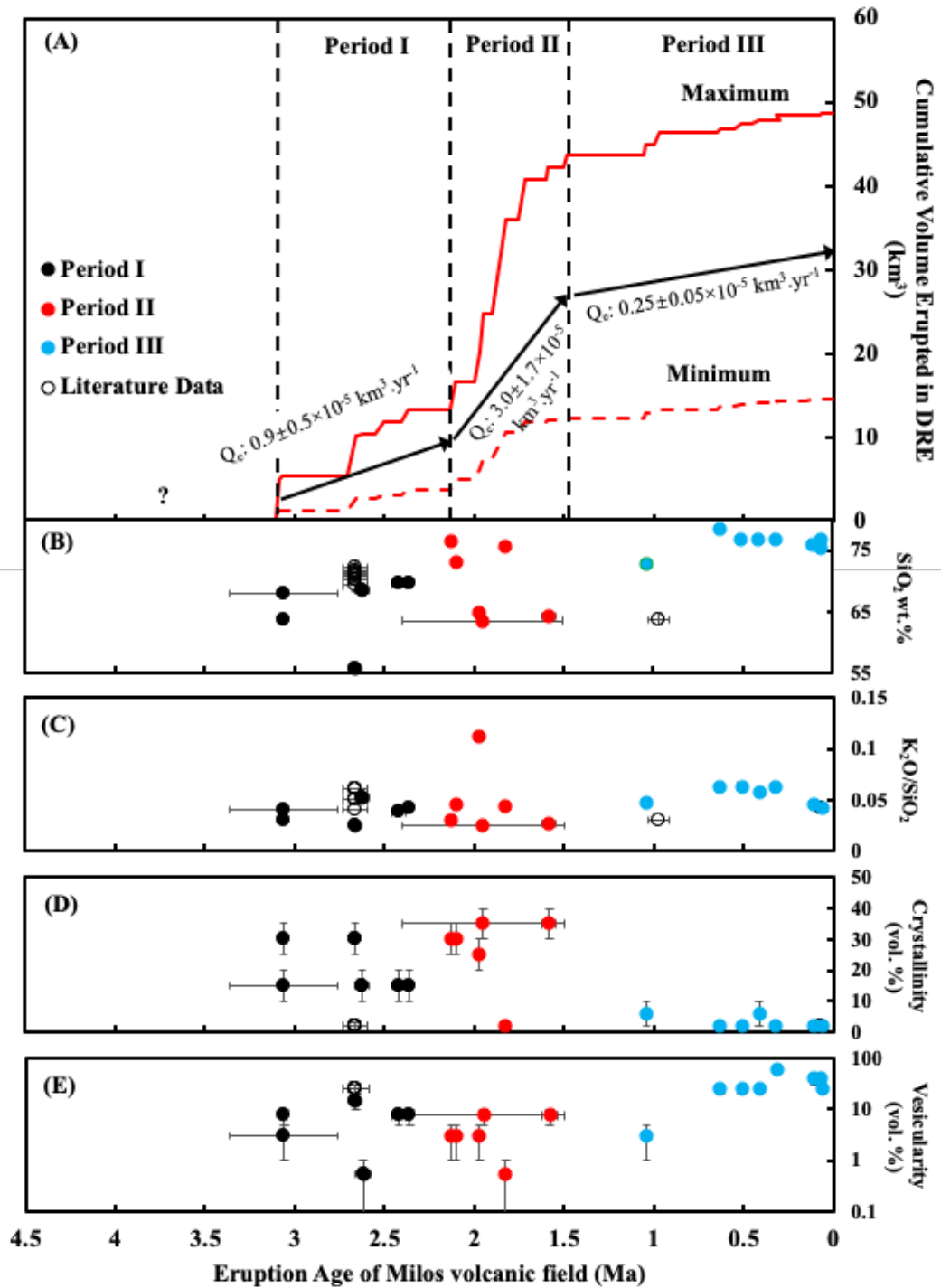
Figure 11. Eruption age versus (A) cumulative eruption volume for the volcanic deposits of Milos, (B) SiO₂ wt.%, (C) K₂O%/SiO₂%, (D) crystallinity vol. % and (E) vesicularity vol. % of Milos volcanic units of this study and previous studies. The maximum (Max; red line) and minimum (Min; dashed red line) cumulative eruption volume curves were estimated from Campos et al. (1996) and Stewart and McPhie (2006). Q_e is the long term volumetric volcanic output rate (see discussion). The exact volume of volcanic products between 4.1 and 3.08 Ma is not well constraint and indicated with a question mark. In this study, the estimations of crystallinity and vesicularity on the older samples (>1.0 Ma) are all from lava and domes. Most of the younger samples (<1.0 Ma) are pumiceous pyroclastic units. The major element, crystallinity and vesicularity data of the old pumices of Filakopi volcanoes (2.66 Ma) are from Stewart (2003). The major element data of the Plakes lava dome is from Fytikas et al. (1986). Geochemical, crystallinity and vesicularity data of the old pumices of the Profitis Illias (~3.08 Ma) is lacking due to the severe alteration.
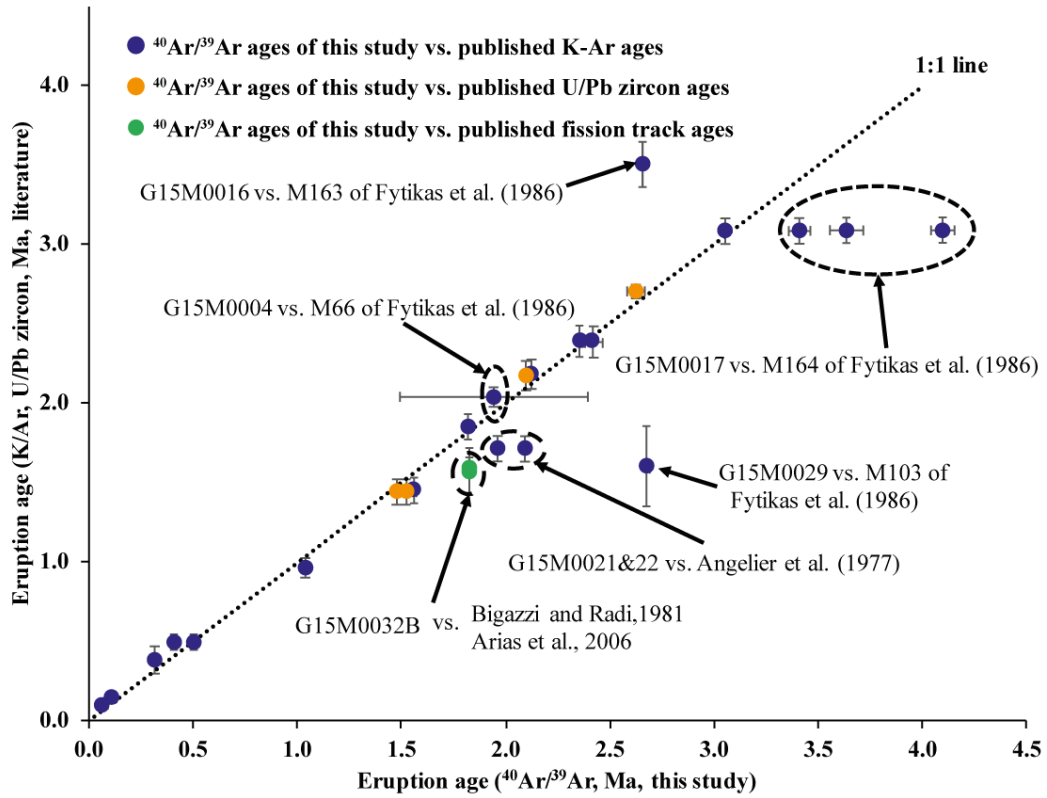
Figure 12. The ⁴⁰Ar/³⁹Ar ages of this study (x-axis) compared to the K/Ar ages (Angelier et al., 1977; Fytikas et al., 1986), U/Pb zircon ages (Stewart and McPhie, 2006) and fission track ages (Bigazzi and Radi, 1981; Arias et al., 2006) (y-axis) for the same volcanic units. Ages which deviate from the 1:1 correlation line are discussed in section 4.1.
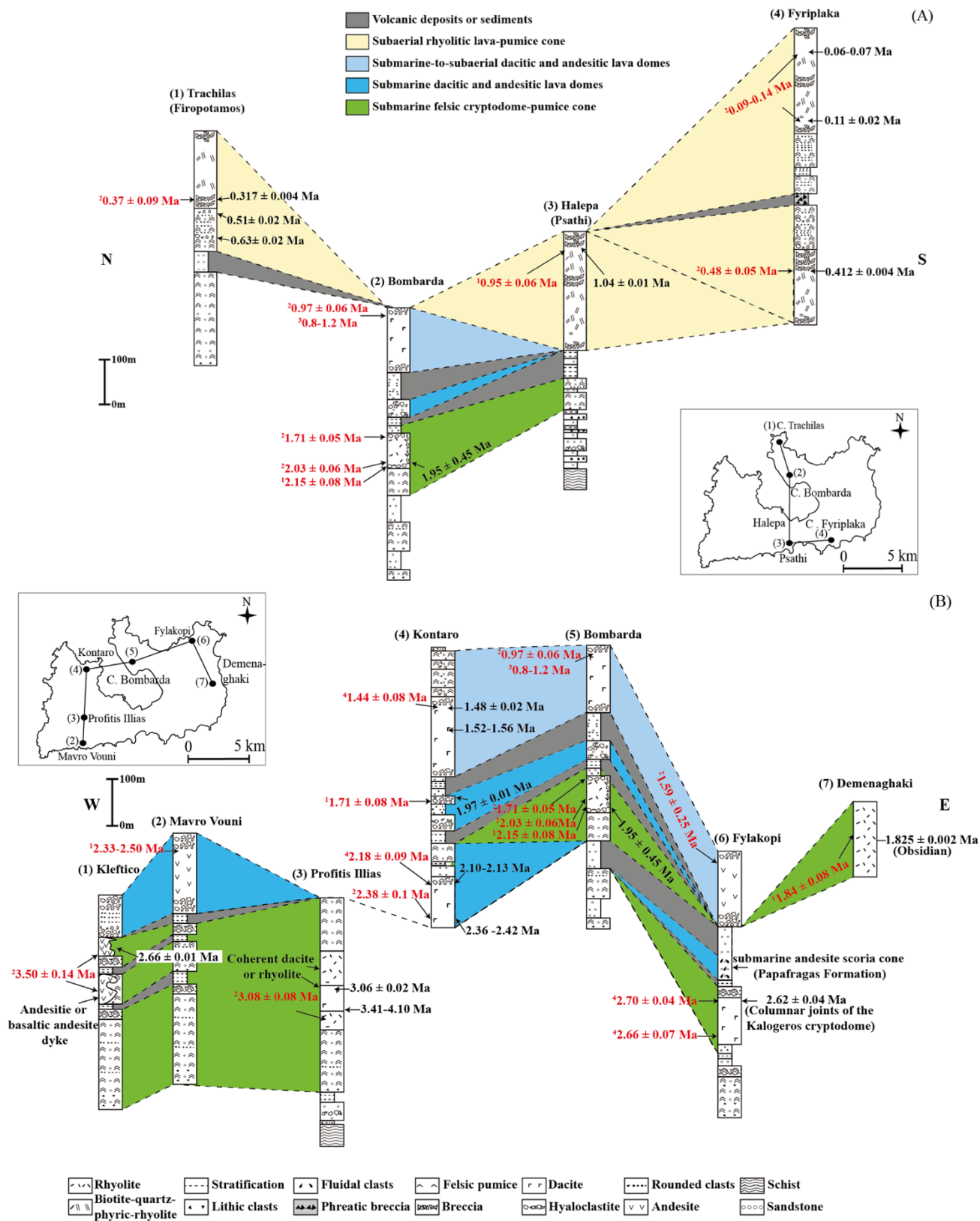
Figure 14. Nine selected stratigraphic columns covering the (A) young (<1.4 Ma) and (B) old (>1.4 Ma) volcanic deposits of Milos modified after Stewart and McPhie (2006), except for (7) Demenaghaki. Age data in black are from this study and in red are from: 1=Angelier et al. (1977), 2=Fytikas et al. (1976, 1986), 3=Matsuda et al. (1999), 4=Stewart and McPhie (2006).
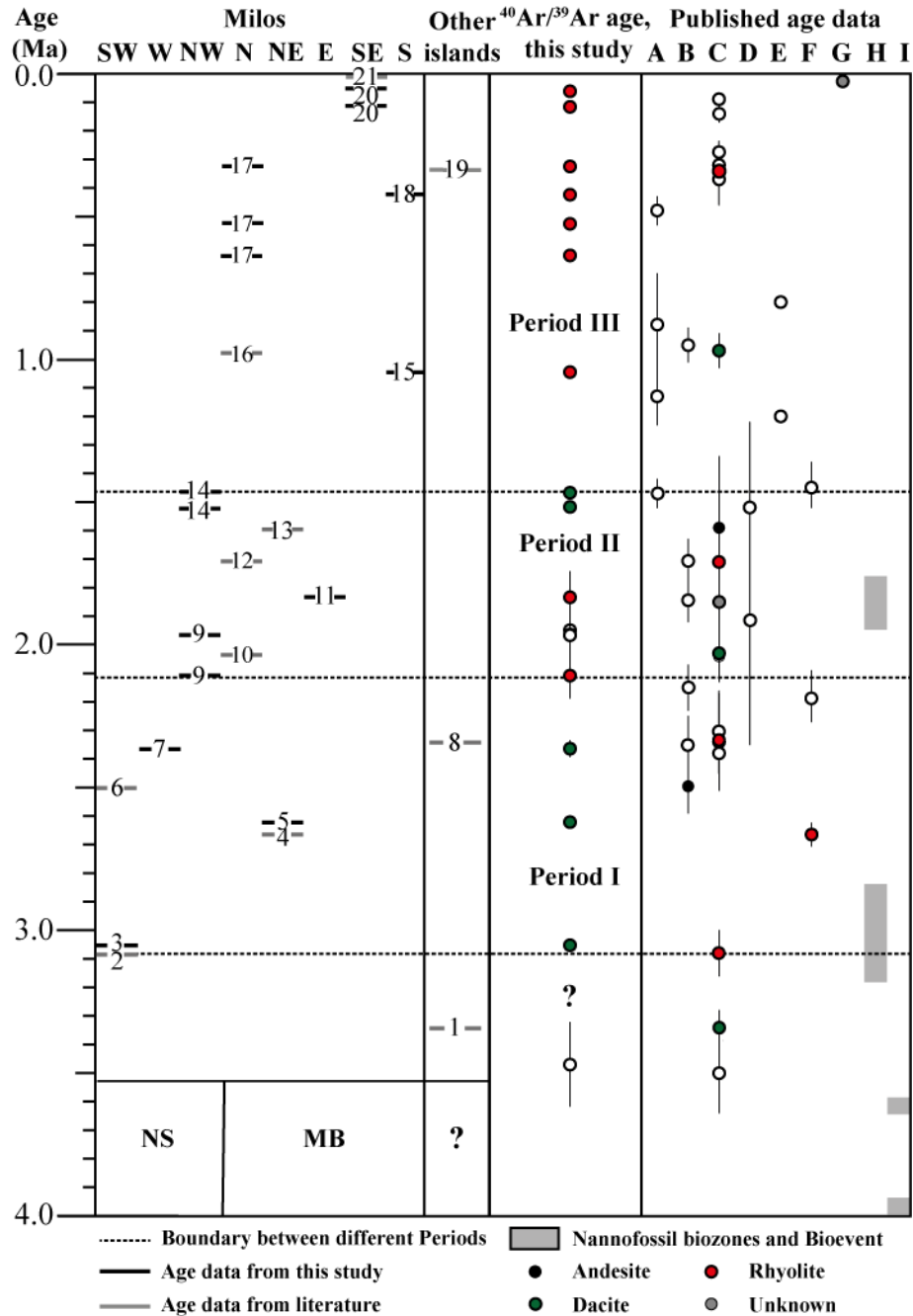
Figure 14. Diagram presenting three periods of different long term volumetric volcanic output rate on Milos volcanic field based on the new $^{40}Ar/^{39}Ar$ data of this study and published data. The location of the different volcanoes is given in Fig 2 and indicated in the left panel (from left to right: SW, W, NW, N, NE, E, SE and S of Milos). The right panel corresponds to published age data: [A]=Fytikas et al., 1976, [B]=Angelier et al., 1977, [C]=Fytikas et al., 1986, [D]= Bigazzi & Radi, 1981, [E]=Matsuda, 1999, [F]=Stewart and McPhie (2006), [G]= Trainau and Dalabakis, 1989, and Biostratigraphic data of the Neogene sediments (NG) is from [H]=Calvo et al. (2012) and [I]=Van Hinsbergen et al. (2004) calibrated to Raffi et al. (2020) (LCO of Sphenolithus spp. and FO of D. tamalis). The number in the left panel represents the volcanic centres of Milos (see details in Table 5). The start of volcanism (3.08-3.61 Ma) on Milos and the basement of the other Islands (Antimilos, Kimolos and Polyegos) are not well constraint and indicated with question marks (see text for discussion). The simplified basement cross-section (NS: Neogene sedimentary rock; MB: Metamorphic basement) under Milos volcanic units is based on Fytikas et al. (1989). We used the filled symbols as the best estimate for the eruption ages at the different volcanic centres.